ELSEVIER

Contents lists available at ScienceDirect

Materials Today Energy

journal homepage: www.journals.elsevier.com/materials-today-energy/



Graphene and its derivatives in lithium-sulfur batteries

Yunya Zhang, Zan Gao, Ningning Song, Jiajun He, Xiaodong Li*

Department of Mechanical and Aerospace Engineering, University of Virginia, 122 Engineer's Way, Charlottesville, VA 22904-4746, USA



ARTICLE INFO

Article history: Received 14 March 2018 Received in revised form 22 May 2018 Accepted 3 June 2018

Keywords: Lithium sulfur battery Graphene Graphene oxide Energy storage Polysulfide

ABSTRACT

On the edge of impending energy and environmental crisis, electrochemical energy storage has rapidly gained momentum. Among all the candidates in the "beyond lithium-ion battery" arena, lithium-sulfur (Li-S) battery has attracted extensive attention due to its ultrahigh theoretical capacity and the abundance of sulfur. However, the development of Li-S battery is hindered by its quick capacity decay and short lifespan because of the insulating nature of sulfur/Li₂S and the high solubility of lithium polysulfides. Under this scenario, graphene and its derivatives have been explored to overcome the shortcomings of Li-S batteries. Graphene is mechanically robust, highly flexible, and exceptionally conductive, enabling abundant porosity for high sulfur loading, expeditious electron/ion transfer, and effective polysulfide encapsulation, Graphene oxide (GO), on the other hand, is often attached with various functional groups which are able to chemically bond with polysulfides, rendering GO a strong polysulfide entrapping ability. The graphene/GO enabled physical confinements and chemical interactions can be further enhanced via constructing graphene-sulfur configurations and doping functional groups or heteroatoms. In addition to the intrinsic advantages, graphene and GO are highly compatible with many engineering materials, making graphene-based composite electrodes promising for low-cost, high-performance Li-S batteries. This review article sequentially illustrates the interaction between sulfur/polysulfides and graphene, sulfur infiltration methods, sulfur/graphene configurations, applications of graphene and its derivatives in Li-S batteries, and presents state of the art and future outlook.

© 2018 Elsevier Ltd. All rights reserved.

1. Introduction

Electrochemical energy storage devices are playing increasingly critical roles. Although oil exploitation techniques have made a notable progress in the past decade, fossil fuel depletion and environmental issues, such as climate changes and air pollutants, are undeniable facts [1]. On the edge of impending energy and environment crisis, a rational and feasible solution is to exploit sustainable energy sources, such as wind, solar energy, and biological energy [2]. However, sustainable energy sources are often intermittent and decentralized, thereby requiring stable, high capacity energy storage systems. As one of the heavily used transportation tools that consume fossil fuel the most, traditional engine-powered vehicles produce a tremendous amount of greenhouse gases and dust particles, which are considered a major reason for global warming [3]. Thusly, an appeal of replacing current combustion engines with more environmentally friendly

revolutionized human society in the past two decades. The "rocking chair" reaction mechanism renders Li-ion batteries outstanding stability and power density [9]. Unfortunately, currently commercialized cathode and anode materials for Li-ion batteries are plagued with low theoretical capacity (LiCoO₂ with a capacity of 270 mAh/g and LiPFeO₄ with a capacity of 170 mAh/g). The most advanced Li-ion batteries are approaching their maximum poten-

power systems is becoming more intense than before [4]. However, the current battery systems with 6 h charging can only support

about 300 mile cruise for electric vehicles [5]. More importantly,

the average cost of the current battery pack is ~\$350 per kWh,

which is far beyond the target affordable price for electric vehicles

(~\$100 per kWh) [6]. Furthermore, lack of high-performance en-

ergy storage systems has become a major roadblock for the

development of portable electronic devices. Next generation always-on and portable electronic devices call for high-

performance batteries with a longer lifespan, higher capacity,

more environmental robustness, and extra functions such as being

flexible and self-healing [7,8]. Lithium-ion (Li-ion) battery has

tial [10–12]. Clearly, Li-ion batteries cannot fulfill the urgent needs

for large-scale grids and electric vehicles which require long time

^{*} Corresponding author. E-mail address: xl3p@virginia.edu (X. Li).

operation and/or high performance/weight ratio [13–15]. To overcome the aforementioned bottlenecks, efforts have been made to enhance the electrochemical performance of Li-ion battery system by replacing graphite anode with Si or Sn [16,17], developing new cathode materials [18], and exploring better electrolytes [19]. On the other hand, people have turned their attention to new battery systems with different reaction mechanisms [6,14].

Among all the candidates under the "beyond Li-ion battery" arena, lithium sulfur (Li-S) battery has attracted extensive attention and is considered as one of the most promising successors for Li-ion battery [20-22]. When sulfur couples with lithium metal anode, a complete conversion between sulfur and its lithiated product Li₂S delivers an ultra-high capacity of 1650 mAh/g, which is 6 times higher than LiCoO₂. Considering the average voltage of 2.2 V vs. Li/Li+, the theoretical energy density of Li-S reaches 2600 Wh/ kg [23-25]. A fully packed Li-S battery is expected to deliver a specific energy of 400–600 Wh/kg, two times higher than the most advanced Li-ion batteries [21,26,27]. Li-S battery system also carries additional assets, such as low cost and environmentally friendly. However, Li-S battery suffers several problems that severely hamper its commercialization (Fig. 1). Firstly, both sulfur and Li₂S are insulating, leading to the low utilization of active materials. Secondly, intermediates between sulfur and Li₂S (Li₂S₈, Li₂S₆, and Li₂S₄) are highly soluble in organic electrolyte, causing "shuttle effect" which deteriorates both anode and cathode [28,29]. Thirdly, the conversion between sulfur and Li₂S results in over 70% volume change, inducing cracks and pulverization in the cathode. To address the aforementioned challenges, an accessible and effective approach is to incorporate sulfur or Li₂S with a scaffold constructed with conductive materials such as conductive polymers, carbon materials, and metal compounds. A qualified scaffold should have an intimate connection with sulfur, possess porous architecture to enhance sulfur loading and encapsulate polysulfides, and be flexible to buffer volume fluctuation [30–32].

Intriguingly, one material that satisfies all the aforementioned requirements is graphene – a single layer of sp^2 bonded carbon atoms [39.40]. So far, graphene its derivatives has been widely used in various fields and exhibited outstanding performances [41–46]. Graphene sheets are usually fabricated by mechanical exfoliation or chemical vapor deposition (CVD) [47,48]. Graphene oxide (GO), as the most important graphene derivative, is often prepared by Hummer's method [49-52]. Graphene and GO are gifted unique properties which are especially beneficial for Li-S batteries (Fig. 1). Graphene is prestigious for its exceptional conductivity [53], which can effectively facilitate the electron transfer for insulating sulfur/ Li₂S. Graphene's outstanding mechanical robustness and flexibility [54] are able to buffer the large volume fluctuation during charge/ discharge and facilitate the fabrication of flexible devices [55]. Its ultra-high specific area (2630 m²/g) [56] empowers grapheneconstructed scaffolds with superlative porous architecture for sulfur loading and redox. GO sheets, on the other hand, are often attached with numerous functional groups which tend to chemically interact with polysulfides, offering a strong entrapping ability [57–59]. In addition to their intrinsic properties, graphene and its derivatives can be functionalized or doped with functional groups or heteroatoms, further enhancing their polysulfide immobilizing ability. Moreover, graphene and GO are highly compatible with many engineering materials such as metal components, carbon

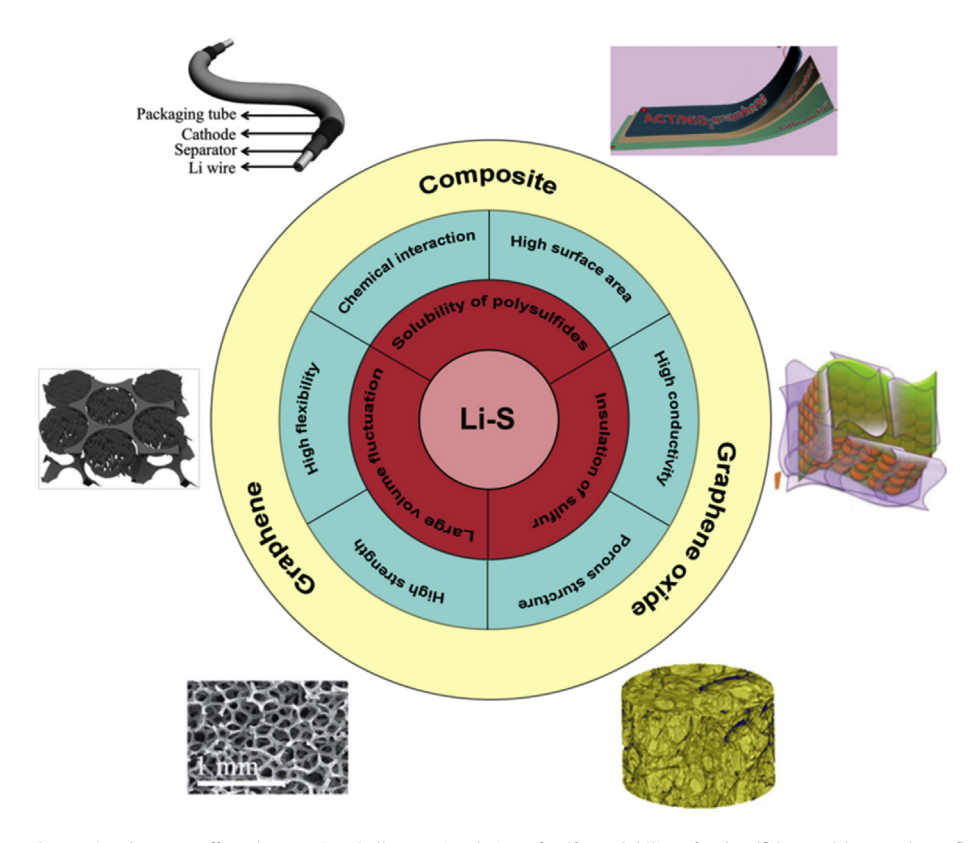


Fig. 1. Li—S battery and graphene. Li—S battery suffers three major challenges: insulation of sulfur, solubility of polysulfides, and large volume fluctuation. Graphene and its derivatives are a perfect solution for these problems. Graphene and graphene oxide (GO) are mechanically robust and flexible, so they can buffer the large volume change. High specific area and functional groups are able to encapsulate and immobilize polysulfides, thereby reducing shuttle effects. The high conductivity of graphene and reduced GO (rGO), as well as their constructed porous structures lay the foundation for outstanding electron and ion transferability, enabling higher utilization of active material. Graphene and its derivatives also have the potential for further development, such as doping, functionalization, and compositing with other materials, including metal components, carbonaceous materials, and conductive polymers. Images reproduced from Refs. [33—38].

materials, and conductive polymers. Graphene and its derivatives have been heavily employed to enhance the electrochemical performance of Li—S batteries [46,60,61] and hold promises in removing the roadblocks (the inevitable anode degradation and the actual low energy density) on the way of commercialization of Li—S batteries [21].

This review will start with the interactions between graphene/ GO and sulfur/polysulfides, followed by sulfur infiltration methods, sulfur/graphene configurations, their applications in Li—S batteries, and a brief summary.

2. Interactions between sulfur and graphene

Sulfur/polysulfides can interact with graphene and its derivatives physically and chemically. The physical interaction stems from the geometrical feature and molecular structure of graphene. Macroscopically, graphene and its derivatives are flexible 2D materials which are able to encapsulate sulfur particles (Fig. 2a) [62]. Such configuration facilitates the electron transfer between insulating sulfur and electrolyte, entraps the dissolved lithium polysulfides, and buffers the large volume change between sulfur and Li₂S, thereby enhancing active material utilization, mitigating shuttle effect, and protecting the cathode from fracture and

pulverization. Microscopically, graphene has a hexagonal honeycomb crystal structure with carbon—carbon sp² bonds connecting each atom and π/π^* bonds orientating out of the plane (Fig. 2b) [63]. Such highly symmetric bonding configuration leads to the non-polar nature of graphene. Intriguingly, element sulfur S₈ has a double layered, octagonal structure, which is also symmetric and non-polar. The non-polar/non-polar configuration results in strong van der Waals' interaction and superior wettability between graphene and melted element sulfur, leading to an extremely small contact angle (Fig. 2c) [63]. The outstanding wettability facilitates infiltration of sulfur into the scaffolds constructed with graphene and its derivatives. However, the hexagonal structure lacks out-ofplane interactions as such van der Waals' force is the only interaction route between graphene and sulfur/lithium polysulfides [64]. The weak interaction often results in poor immobilization of polysulfides. Comparing with perfect graphene, defective graphene exhibits stronger van der Waals' force with sulfur [64]. Cathode performance can be enhanced by introducing defects in graphene, such as vacants, heteroatoms, and edges on graphene sheets.

The chemical interaction mainly results from the functional groups attached to graphene sheets. GO, which is also called graphitic acid, is usually prepared by Hummer's method [49–52], in which strong oxidizing agents (H₂SO₄, HNO₃, KMnO₄, H₃PO₄) are

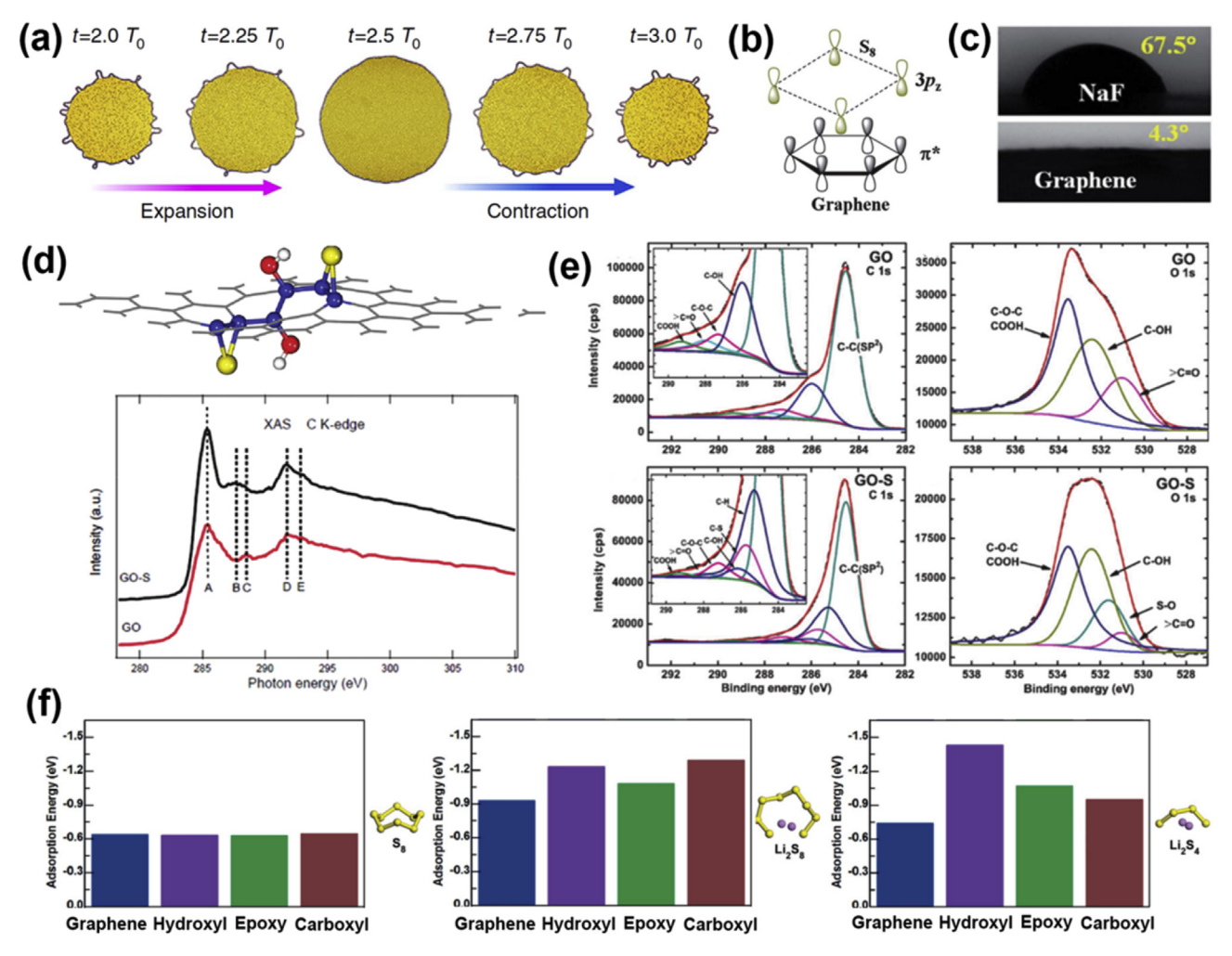


Fig. 2. Interactions between sulfur and graphene/GO. (a) Graphene and GO are able to encapsulate sulfur particles, thereby enhancing electron transfer, entrapping the dissolved polysulfides, and buffering the volume change [62]. (b) Both graphene and element sulfur have symmetrical, non-polar structure [63]. (c) The wettability between graphene and sulfur is outstanding [63]. (d) Sulfur can bond with the functional groups on GO, leading to a stronger chemical interaction [65]. (e) XPS spectra illustrate that C–S and O–S bonds formed after sulfur infiltration [66]. (f) Oxygen functional groups have no major influence on the adsorption of S₈ but strongly effect the adsorption of polysulfides. Hydroxyl functions have the strongest interaction with Li₂S₄ and carboxyl functional groups have the strongest interaction with Li₂S₈ [67]. Images reproduced from Refs. [62,63,65–67].

used to forcibly insert between graphene layers in graphite and break the van der Waals' bonds. Because of such violent method, comparing with graphene, GO is highly defective, containing a large amount of chemical (functional groups) and structural (vacants and voids) defects [59]. In addition to carbonyl (C=0) and oxygen atoms (=0), epoxy, hydroxyl (-OH), carboxyl (-COOH), and phenol were also found on the graphene sheets [59]. The functional groups. mainly hydrogen containing groups such as hydroxyl and carboxyl, can be entirely or partially removed by thermal or chemical reductions. The reduced product, which is the so-called reduced GO (rGO), shows relatively higher conductivity, more mechanical robustness, and even higher defectiveness than GO [58]. The functional groups and defects, although deteriorate the conductivity and mechanical properties of graphene, render GO several unique properties. Firstly, GO is hydrophilic and hence dispersible in water and other solvents, such as liquid methanol, ethanol, and acetone. The hydrophilic nature not only reduces the tendency of restacking and aggregation, but also can be used for fabricating hierarchically porous structures. Secondly, sulfur can be incorporated with GO via multiple liquid methods, increasing sulfur loading and promoting homogenization. Finally, the most important advantage of GO for Li-S batteries is that the functional groups enable strong chemical interactions with lithium polysulfides, effectively entrapping and immobilizing them and largely reducing the shuttle effect. Soft X-ray absorption spectroscopy (XAS) inspection revealed that both epoxy and hydroxyl groups interacted with sulfur (Fig. 2d) [65]. X-ray photoelectron spectroscopy (XPS) discovered C-S and O-S bonds in a GO/S cathode (Fig. 2e) [66]. suggesting that sulfur was chemically bonded to the GO. The incorporation of sulfur with GO demonstrated only a weak influence on the electronic structure of carbon but a considerable impact on the density of the occupied O 2p configurations, indicating that sulfur mainly reacted with the functional groups other than the carbon atoms [66]. Density functional theory (DFT) calculations [36] revealed that substantial binding occurred between the oxygen-containing groups and sulfur/polysulfides, especially S₃ anions. Kimal Chandula Wasalathilake et al. further investigated interactions between sulfur, polysulfides, and graphene. Oxygen functional groups have no major influence on the adsorption of S₈ but strongly affect the adsorption of polysulfides. Hydroxyl functions have the strongest interaction with Li₂S₄ and carboxyl functional groups have the strongest interaction with Li₂S₈ (Fig. 2f) [67].

Both physical and chemical interactions can be further enhanced by reforming and/or redeveloping graphene and GO. Rational design of graphene scaffold architectures can enhance the physical encapsulation. Various methods, such as hydrothermal annealing, CVD, templating, and acid/alkane etching, were employed to construct hierarchically porous structures on graphene/GO substrates. The micropores, with a pore size smaller than 2 nm, are able to affect the kinetics of S₈ dissolution process [68] and restrain the diffusion of polysulfide chain [69,70]. The van der Waals' force has a significant increase of adsorption strength as the pore size decreases from 1 nm to 0.75 nm, thereby improving the cyclic stability of Li–S batteries [67]. The mesopores (pore sizes ranging from 2 to 50 nm) have strong physical absorption of sulfur and polysulfides, increasing the utilization of active materials and improving specific capacity [32,71,72]. The macropores (pore sizes larger than 50 nm), on the other hand, have little influence on polysulfide confinement, but can improve sulfur loading, buffer volume change, and enhance electrolyte accessibility [73–75]. Two major approaches are often used to improve the chemical interactions: doping and functionalization. Many heteroatoms such as N [76,77], S [78], P [79], I [80], and B [81], were doped or codoped onto graphene and its derivatives. The doped heteroatoms are able to form bonds with sulfur and polysulfides, doubling or even tripling the bonding energy [21,82]. Functional groups such as catecholamine [83], amino [26,84], phenyl sulfonate [85], oleylamine [68], and sulfhydryl [86] were implanted into graphene sheets to improve the bonding energy between graphene/GO and lithium polysulfides. The functionalization is often conducted in liquid under mild conditions, making the fabrication of functionalized graphene sheets efficient and low-cost.

The strong physical and chemical interactions between graphene/GO and sulfur/polysulfides endow Li-S/graphene batteries outstanding electrochemical performance. In fact, graphene and its derivatives are highly compatible with other materials. If one property of a graphene-based cathode is poor, other materials can be feasibly composited with the cathode to compensate the weakness. For instance, the conductivity of GO is deteriorated by defects and functional groups for strong chemical interactions, carbon nanotubes (CNTs) can be incorporated into the cathode to improve its conductivity such that the GO/CNT/S hybrid cathode achieve simultaneously high electron transfer ability and polysulfide entrapping ability [87,88]. When the physical interaction and conductivity are maximized by defect-free graphene, the chemical interaction is often compromised; materials with stronger bonding energy with polysulfides, such as metal oxides [89] and metal-organic frameworks (MOFs) [90], are wisely incorporated to overcome the shuttle effect. Such tunability opens up unprecedented opportunities for graphene and its derivatives in Li-S battery and other energy storage systems.

3. Sulfur infiltration

The superior chemical stability and ultrahigh wettability with sulfur enable smooth infiltration of sulfur into graphene-based scaffolds. Sulfur infiltration methods can be grouped into three room-temperature mechanical mixing, categories: temperature anneal, and solution-based processing. The first method is to mix sulfur with graphene/GO mechanically, often by ball milling, which is low-cost, feasible, and efficient. However, it is still challenging for such mechanical method to achieve high homogeneity and strong bonding between sulfur and graphene/GO [91]. High-energy, long-time ball milling may stimulate the reaction between sulfur and graphene edges, leading to a stronger immobilization for polysulfides [92]. The second approach - hightemperature infiltration - is to infiltrate sulfur at around 155 °C when sulfur has the lowest viscosity [93]. The molten sulfur can infiltrate into small pores, even nanosized pores. The two-stage annealing sulfur infiltration vaporizes the excessive sulfur segregated on the surface, leading to a better dispersion [94]. This method is environmentally friendly. Transmission electron microscopy (TEM) inspection [74,95] unveiled that sulfur carried the form of nano crystals on the graphene sheets after the two-stage annealing, facilitating electron transfer and improving the utilization of active materials. However, the amount of sulfur infiltrating into the graphene scaffold is dependent on the porosity because the exposed sulfur will be vaporized during annealing, making the sulfur content and sulfur loading difficult to control.

The solution-based processing is to composite sulfur with graphene sheets in a liquid solution. Sulfur has a highly symmetric structure such that it is not dissolvable in polar solvents, such as water. However, sulfur can be dissolved in non-polar solvents, especially CS₂. Thusly, a simple and straightforward method is to infiltrate sulfur dissolved CS₂ into the porous graphene scaffold or directly stir the solution with graphene/GO flakes and then vaporize CS₂, leaving sulfur on the graphene surface [36,96,97]. Since the solubility of sulfur in CS₂ is very high and the evaporation process can be repeated several times, the amount of sulfur can be accurately controlled. However, CS₂ is volatile and toxic. Another

approach is to take advantage of the depositing reaction between sulphureous salts and/or hyposulfite salts and acid:

$$S_x^{2-} + 2H^+ \rightarrow (x-1)S + H_2S$$
 (1)

$$S_2O_3^{2-} + 2H^+ \rightarrow S + SO_2 + H_2O$$
 (2)

$$2S^{2-} + S_2O_3^{2-} + 6H^+ \rightarrow 4S + 3H_2O$$
 (3)

In this route, sulfur-containing salts, normally Na₂S or Na₂S₂O₃, were dissolved in water and mixed with graphene. Diluted acid solutions, such as HCOOH or HCl, were then added to the slurry, stimulating the precipitation and segregation of sulfur on the graphene flakes [65.98–100]. This route has been widely used because it is safe and environmentally benign and the sulfur content is controllable. Except for the aforementioned two liquid-based methods, other approaches have also been explored. A hydrothermal method is to seal GO with sulfur suspension in an autoclave to anchor nano sulfur particles on the graphene sheets [101,102]. A reverse microemulsion method was employed to composite graphene with sulfur, which achieved an ultra-high sulfur content of 94% [81]. Another interesting process is to bubble H₂S gas into GO suspension to simultaneously reduce GO and composite sulfur with rGO to produce rGO/S cathode while reducing H₂S pollution [103,104]. One other alternative route is to mix rGO sheets with sulfur-ethylenediamine anhydrous (S-EDA) precursor to realize sulfur infiltration with a controllable sulfur particle size of 5 nm [105]. Table 1 lists brief procedures and respective advantages/ disadvantages of the aforementioned sulfur infiltration methods. Worth mentioning is that all the methods discussed are not mutually exclusive. They can be used together to enhance sulfur infiltration and dispersion. For instance, the high-temperature anneal is often used after liquid-based processing to promote sulfur infiltration into graphene scaffolds [36,80,84].

In addition to sulfur, lithium sulfide (Li₂S) was also used to composite with graphene for Li–S batteries [106,107]. Two distinct advantages of using Li₂S instead of sulfur are: (1) the cathode mechanical damage due to the volume expansion can be reduced because Li₂S is fully lithiated and occupies the maximum volume compared with sulfur and other lithium polysulfides; (2) the melting temperature of Li₂S (1372 °C) is much higher than that of sulfur (115 °C) such that high-temperature treatments can be conducted without any loss of the active material. A simple dropcoating method was used to composite Li₂S nanoparticles with

rGO paper [108]. Recently, Li₂S was encapsulated into rGO shell via the reaction between sulfur and lithium triethylborohydride ((LiEt₃BH) [109]. A Li₂S₆/GO precursor was also used to construct Li₂S/rGO cathode by high-temperature annealing [110]. However, in addition to its lower theoretical specific capacity (1166 mAh/g), the low electron conductivity and dissolution of polysulfides are unable to be suppressed by replacing sulfur with Li₂S.

4. Sulfur/graphene configurations

Various graphene/sulfur configurations have been exploited to maximize the utilization of active materials and facilitate the electron/ion transfer. As illustrated in Table 2, after sulfur infiltration, graphene/sulfur configurations can be grouped into five categories: in-plane, sandwich, core—shell, 3-D, and the combination of thereof. In-plane means that sulfur is directly deposited on graphene sheets and the composite is then used as an electrode without further treatment [105,111,112]. In this configuration, sulfur and polysulfides mainly bond with graphene and its derivatives via defects, pores, and functional groups. Such in-plane structure does not provide enough physical encapsulation for sulfur/polysulfides. However, if the chemical interaction is strong, this configuration can offer exceptional sulfur/graphene utilization. A solution to enhance the physical encapsulation is to confine sulfur in between two layers of graphene, forming C/S/C sandwich-like structure [63,97]. Such configuration not only increases polysulfide encapsulation but also enables excellent electron transfer. However, the dissolved polysulfides may still leak out from the graphene edges and the sulfur at the center is not able to participate in the reaction in a timely manner, leading to an active process with the preceding of cycling [113]. The third configuration, as being named "coreshell", describes that sulfur particles are wrapped with graphene and its derivates [100,114], a good example of utilizing the flexibility of graphene. Three unparalleled advantages of such core-shell architecture are (1) outstanding lithium polysulfide entrapment. (2) excellent volume buffering capability, and (3) high sulfur loading, making this configuration promising for the commercialization of Li-S batteries. However, the electron transfer in the core-shell structure is weaker than the in-plane and sandwich structure because the center of sulfur particle only contacts with the graphene walls until the periphery of the sulfur particle is fully reacted. By lyophilizing graphene hydrogel, hierarchically porous GO foam, often called 3-D graphene, was fabricated [36,115]. Such interconnected porous GO foam renders high sulfur loading

 Table 1

 Sulfur infiltration methods and respective advantages and disadvantages.

Methods	Procedures	Advantages	Disadvantages
Mechanical mix	Ball mill graphene sheets with sulfur powders	Low-cost, feasible, and efficient	Hard to achieve high homogeneity and strong bonding
High temperature annealing	Anneal sulfur/graphene mix at 140–160 $^{\circ}$ C and then 180–220 $^{\circ}$ C	High sulfur homogeneity and environmentally friendly	Hard to control the amount of sulfur
CS ₂ evaporation	Dissolve sulfur into CS ₂ and then evaporate CS ₂ solvent	Simple and can repeat several times, enabling controllable sulfur amount	CS ₂ is volatile and toxic
Sulphureous salts and/or hyposulfite salts and acid reaction	Disperse graphene flakes into Na_2S or $Na_2S_2O_3$ solution and then add diluted acid solutions, such as HCOOH or HCl	Safe, environmentally benign, good sulfur homogeneity, and controllable sulfur content	Sulfur dispersion and particle size are highly dependent on the experimental parameters
Hydrothermal treatment	Disperse graphene flakes in solvents and seal with sulfur in an autoclave, and then heat at a temperature of $90-160^{\circ}\text{C}$	Good sulfur homogeneity and controllable sulfur particle size	Not suitable for scale-up production
H ₂ S reduction	Bubble H_2S into the GO suspension while stirring at 70 $^{\circ}C$	Reduce GO and deposit sulfur at the same time	Involve gas preparation and gas transfer
Reverse microemulsion Sulfur-amine precursor	Mix an organic oil phase solution with an aqueous solution Drop Sulfur-ethylenediamine anhydrous (S-EDA) precursor in to graphene/ethanol solution.	Achieve high sulfur loading, good sulfur homogeneity, and small sulfur particle size	Relatively complex procedures which may increase the cost

Table 2 Sulfur/graphene configurations and respective advantages and disadvantages. Images reproduced from Refs. [35,62,63,36,97,100,111,112,114,115].

	Schematic diagrams	Microstructure	Advantages	Disadvantages
In plane	\$ \$ \$ \$ \$ \$ \$ \$ \$ \$ \$ \$ \$ \$ \$ \$ \$ \$ \$	a) all nin	High graphene utilization efficiency	Weak physical encapsulation for sulfur/polysulfides
Sandwich	Will Trees.		Excellent electron transfer	Dissolved polysulfides may leak out from the graphene edges
Core-shell		(b) Uniquin	Outstanding polysulfides entrapment, high sulfur loading excellent volume buffering capability	Relatively sluggish electron transfer for the center of sulfur particles
3-D			High sulfur loading and outstanding electrolyte accessibility	Require extra electrolyte and relatively low graphene utilization efficiency
Combination			Advantages from two kinds of configurations	More complex procedures and higher usage of graphenes

and outstanding electrolyte accessibility. However, the estimated high energy density is in fact compromised by the extra mass of electrolyte and electrode, weakening the overall performance. Thusly, each graphene/sulfur configuration has its own advantages and disadvantages. Some researchers integrated two or more configurations [35,62]. For instance, a graphene scaffold constructed by combining sandwich structure with core—shell structure exhibited a joint enhancement of rate ability and cyclic capability, indicative of outstanding polysulfide entrapment and electron/ion conductivity [35]. However, combining two or more configurations usually requires more complicate processes and higher consumption of graphene, inevitably increasing the cost and reducing energy density.

5. Applications of graphene and its derivatives in Li—S batteries

5.1. Graphene for Li-S batteries

In this section, graphene indicates defect-free graphene sheets derived from mechanical exfoliation, CVD, or ultrahigh-temperature annealing and their redeveloped products. Without functional groups and defects, pristine graphene exhibits distinct advantages and disadvantages: outstanding conductivity and weak polysulfide entrapping ability. When sulfur is composited directly with untreated graphene sheets [63,116—118], the assembled batteries often displayed low specific capacity, fast capacity decay, and/or rapid capacity decrease in the first several cycles. This indicates that dissolved polysulfides were not encapsulated and immobilized, leading to an irreversible capacity loss. Multiple methods have been jointly used to enhance the physical and chemical

interactions between graphene and lithium polysulfides. The first approach is to construct porous structures. Unlike GO, defect-free graphene sheets are not solvable; thereby templates and precursors are widely used in constructing porous scaffolds. Nickel foams were employed as templates to fabricate 3D layered graphene foams by CVD method [37]. The obtained graphene scaffolds exhibited intriguing interconnected architecture and outstanding conductivity (Fig. 3a). However, fabricating nano/mesopores by using metallic templates is still challenging. Templates from metal oxides and metal hydroxides have thusly been explored. CaO plates [119], MgO microrods [120] (Fig. 3b), and MgO plates [121] were exploited to fabricate hierarchically porous graphene (HPG), vertically oriented porous graphene-like nanosheets (Fig. 3b), and hierarchical carbon nanocages (hCNC). Fe₃O₄ nanoparticle superlattices were employed as templates for ultrathin mesoporous graphitic-carbon frameworks (MGFs) [122]. Layered MgAl double oxide (LDO) flakes [123,124] and layered MgAl double hydroxide (LDH) nanospheres [125] were then explored as precursors to synthesize unstacked double-layer template graphene (DTG), mesoporous graphene frameworks (PGFs), and graphene microspheres (GMSs). Graphene scaffolds fabricated via these methods simultaneously possessed outstanding conductivity and hierarchical pores, rendering outstanding cyclic stability and rate ability. Metal chlorides, on the other hand, are often used to fabricate the core-shell structure. For instance, hollow graphene nanoshells (HGNs) with a diameter of 10-30 nm and a pore volume of 1.98 cm³ g⁻¹ were synthesized by NiCl₂ with sodium dodecyl sulfate (SDS) precursors [71] and hollow nanoporous graphene powders were synthesized via FeCl₃ catalyzed CVD method [126]. The well-organized graphene shells effectively entrapped the dissolute polysulfides and facilitated electron and mass transport. In addition

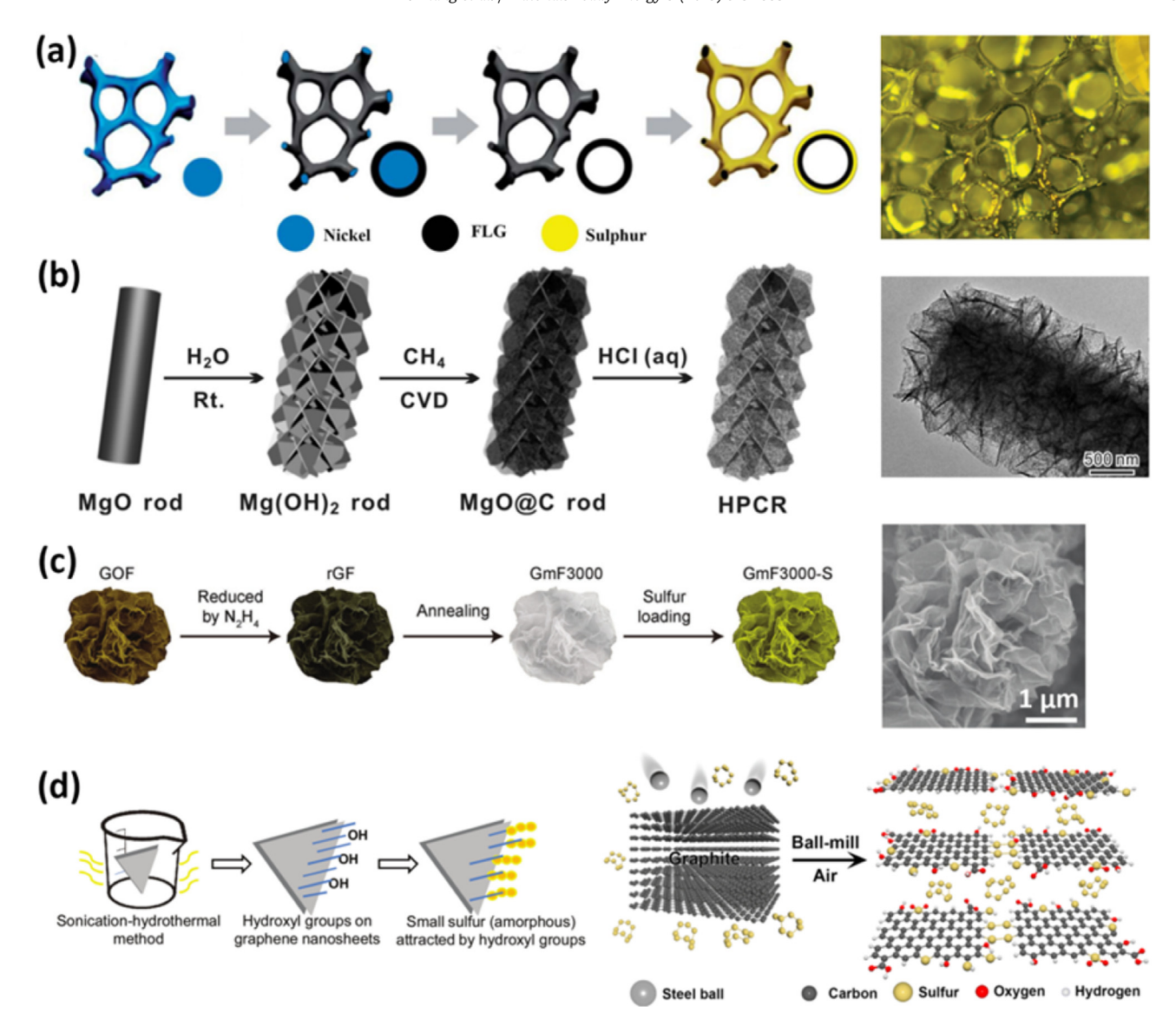


Fig. 3. Porous graphene scaffold construction and graphene functionalization. (a) Graphene foam derived from nickel foam with interconnected micron-sized pores [37]. (b) Hierarchically porous graphene rods fabricated using Mg(OH)₂ precursor [120]. (c) Graphene microflowers produced by reducing GO at ultrahigh-temperature [129]. (d) Hydroxylated and sulfureted graphene nanosheets fabricated by sonication-hydrothermal method and intense ball milling [92,132]. Images reproduced from Refs. [92,37,120,129,132].

to inorganic compounds, organic compounds have been employed as the precursors to construct graphene scaffolds. Metal ion exchanged resin precursors were used to in situ anchor sulfur nanoparticles in three-dimensional (3D) porous graphitic carbon (PGC) and 3-D graphene-like material (GIM) [72.127]. The obtained cathode achieved high sulfur loading with stable cyclic ability. Ultrahydrophilic graphene stacks with highly accessible interlayer nano-sized pores were fabricated by layered MOF templates. The obtained scaffold displayed strong static absorption for dissolved polysulfides [128]. All the aforementioned methods sacrificed the templates to construct nanostructure, which inevitably increases the cost. A high-throughput fabrication method was proposed to synthesize porous crumpled graphene microflowers (GmF) via spray drying and high-temperature annealing at 2000-3000 °C (Fig. 3c) [129]. In another route, caterpillar-like graphene was fabricated and confined sulfur by a restacking effect [130].

The second approach to enhancing the graphene/polysulfide interaction is to dope or functionalize graphene sheet, indicative of implanting heteroatoms or functional groups on the carbon basal

plane. Due to the absence of defects, graphene is more difficult to be doped functionalized than GO or rGO, thereby requiring more sophisticated/severe physical/chemical approaches. For instance, nitrogen atoms were homogeneously doped during CVD process at a temperature of 750 °C [131]. Sonication-hydrothermal method [132], intense ball milling [92], and HF treatment [133] were used to construct hydroxylated, sulfureted, and fluorinated graphene nanosheets (Fig. 3d), which simultaneously retained the conductivity and enhanced the chemical interactions, resulting in better electrochemical performances.

Although the defect-free, pristine graphene has weak polysulfide entrapment and requires more complicated treatments to improve the physical/chemical interactions with polysulfides, the unparalleled conductivity and electron transferring ability render graphene-based cathodes superior rate performance comparing with other carbonaceous frameworks. For instance, the 3D graphene scaffold produced by Ni templates (Fig. 3a) can sustain over 400 cycles at a current density of 3.2 A/g [37]; the HPG derived from CaO precursor exhibited a high capacity retention rate of 74% when the current being density increased from 0.1 C to 5 C [119]; the 3D S@PGC cathode produced by Fe ion exchanged resin maintained a specific capacity of over 400 mAh/g at 5 C rate with high sulfur loading [72]; the vertically oriented porous graphene-like nanosheets synthesized from MgO microrods (Fig. 3b) enabled high capacity at over 5 C rate [120]. According to galvanostatic intermittent titration technique (GITT) studies [68], graphene mainly influences the kinetics of the Li₂S formation process, thereby enhancing the rate ability. However, more outreaching and profound studies are still needed to unveil the fundamental mechanisms of such kinetics improvement.

5.2. GO and rGO for Li-S batteries

Here, GO indicates graphene produced by Hummer's method [49–52]. Unlike defect-free graphene, GO is more versatile, i.e. it has decent conductivity and mechanical properties as well as relatively strong chemical bonding with polysulfides. The hydrophilic nature makes GO dispersible in water, offering the possibility of various liquid-based processes. High-temperature annealing or chemical treatments can partially or mostly remove functional groups on GO, forming reduced GO (rGO). After reduction, the conductivity is restored but the hydrophilic property is eliminated. rGO is even more defective than GO. The properties of GO and rGO are highly tunable via annealing or chemical reductions and can be further enhanced by multiple feasible methods. Because of these unique features, GO and rGO have been extensively used in Li–S batteries.

The hydrophilic nature of GO has been widely exploited for sulfur infiltration. As discussed in Section 3, GO is dispersible in many solvents, thus rendering various liquid-based sulfur infiltration approaches such as CS₂ vaporization [36,96,97], sulfureted salt/ acid reaction [65,98], hydrothermal method [101,102], one pot solution-chemical reaction—deposition [100], H₂S reduction [103,104], and sulfur-amine chemistry, which effectively deposited monodispersed sulfur nanoparticles with controllable sizes on the rGO scaffold [105]. Specifically, sulfur-ethylenediamine anhydrous (S-EDA) precursor was mixed with rGO sheets in water/ethanol mixed solvents. The sulfur-amine complex decomposed, releasing elemental sulfur and forming octatomic S₈ particles on the surface of rGO sheets. The size of sulfur particles was accurately controlled by adjusting reaction parameters. With ultrafine sulfur nanoparticles (5 nm in size) anchored on the rGO sheets, the assembled battery exhibited outstanding sulfur utilization (nearly 100%), rate ability, and cyclic stability, indicating that if the sulfur is confined within nano-sized domains, GO alone is a high-performance sulfur carrier (Fig. 4a) [105].

The hydrophilic nature of GO was also exploited to construct core-shell or 3D structures (Table 2) via room-temperature, liquidbased processes. Molecular dynamics (MD) simulation validated that liquid dispersed graphene sheets tend to be self-assembled into hollow sphere shells or wrap onto particles [134]. GO is often directly wrapped onto sulfur particles. A one-pot water bath reaction by mixing Triton TX-100 aqueous solution, (NH₄)₂S₂O₃, urea, and GO was used to fabricate a well-defined core-shell structure. The assembled Li–S battery exhibited 94.2% capacity retention rate after 500 cycles, indicative of superior polysulfide entrapment [100]. Another route to exploit this property is to construct hollow graphene nanostructures by templating and then infiltrating sulfur into the empty cores [135]. Graphene reinforced graphitic carbon nanocages (G-GCNs) were recently synthesized by ferrous salts precursors [136]. The battery constructed by such G-GCNs exhibited an outstanding lifespan of 1000 cycles with 78.4% capacity retention. The mostly used fabrication procedure of 3D graphene foam is illustrated in Fig. 4b [36]. Specifically, GO sheets are dispersed into a solvent and the GO suspension is then frozen and freeze dried, forming GO foam with interconnected pores. The obtained GO foam is usually compressed and heat treated to decrease the pore size and enhance the conductivity. The interconnected, conductive scaffold often exhibits exceptionally high sulfur loading and excellent electrolyte accessibility, making it an excellent candidate for high sulfur loading electrodes [36,137–141]. For instance, an interconnected fibrous graphene/sulfur cathode fabricated by this method showed a 71% sulfur content and a capacity of 400 mAh/g at 4.5 A/g current density [36]. A free-standing sulfur/three-dimensional graphene framework (3DGF) electrode achieved a high sulfur loading of 90% and operated 500 discharge/ charge cycles with a capacity retention of over 70% [140]. Intriguingly, a dense rGO/S foam fabricated directly by oven drying exhibited a better polysulfide entrapping ability [141]. Another dense rGO/S foam was prepared by H₃PO₄ activation together with the capillary evaporation-induced drying method displayed "inkbottle-like" pores and superior performances [142]. These two studies indicate that there is still room to further improve 3D graphene architectures.

The functional groups on GO sheets have been proven to be capable to bond with lithium polysulfides, thereby reducing the shuttling effect (Fig. 2d-f) [36,65-67]. To further enhance the chemical bonding between GO and lithium polysulfides, one effective approach is functionalization, i.e. grafting functional groups from the organic agents on GO sheets. In one specific study, GO sheets were treated with ethylenediamine (EDA), forming EDAfunctionalized rGO (EFG). The grafted amino groups interacted with polysulfides, preventing the detachment of lithium sulfide from the carbon matrix (Fig. 4c) and thus rendering a capacity retention rate of 80% after 350 cycles with an excellent high-rate response up to 4 C current density [84]. The similar enhanced electrochemical performance was obtained in the cetyltrimethyl ammonium bromide (CTAB) modified S-GO nanocomposite [144], catecholamine functionalized rGO scaffold [83], oleylamine (OLA)-functionalized rGO electrode [68], and vinyl-group-functionalized rGO [145]. Moreover, sulfur-containing functional groups, such as PhSO₃ groups [85] and sulfydryl groups [86], were proven to be able to immobilize lithium polysulfides. The sulfydryl-functionalized rGO (GSH) showed a prominent effect on immobilizing sulfur and suppressing the generation of long-chain polysulfides during both charging and discharging processes, leading to a capacity retention rate of 92.6% after 500 cycles at 1 C rate [86]. Another functionalization route is to treat rGO with KOH, improving the specific area and producing a stronger physical attraction [111,146]. A KOH treated rGO achieved an ultrahigh specific surface of 2313 m² g⁻¹ and pore volume of 1.8 cm³ g⁻¹. The dense nanopores trapped elemental sulfur and intermediate polysulfides during cycling, pushing up specific capacity [111].

The second approach to enhance the chemical bonding is to dope heteroatoms on GO sheets. The defective nature of GO largely promotes the doping processes, even under mild conditions. The doped heteroatoms tend to interact with sulfur and lithium polysulfides, forming corresponding chemical bonds. Nitrogen-doped carbon was first explored as the Li-S cathode host [76]. Heteroatoms including N [76,77,147-149], S [78], P [79], I [80], and B [81,150] have been subsequently exploited. Recently, more fundamental studies were carried out to investigate the mechanisms between doped atoms and polysulfides. Sophisticated quantum chemical calculations and Li NMR spectroscopy unveiled the strong dipole-dipole interaction between Li polysulfides and N-doped graphene originates from the electron-rich donors (e.g., pyridinic nitrogen (pN)), and is enhanced by the inductive and conjugative effect of scaffold materials with p-electrons (e.g., graphene) [151]. Huadong Yuan et al. further proven that pyridinic N atoms have the strongest interaction with polysulfides (Fig. 4d) and also act as active sites to decrease the activation barriers for Li₂S decomposing [143]. Double or triple doping further strengthened the performance [21,82,152]. A nitrogen/sulfur co-doped graphene sponge was used as the sulfur carrier where S and N groups were bonded with polysulfides, effectively mitigating the shuttle effect. The assembled battery with graphene coated separator achieved a high sulfur loading of 8.5 mg/cm² with a stable lifespan of 200 cycles [82]. Worth mentioning is that functionalization and doping on GO and rGO are much easier than those on the graphene because their defective nature induced a large number of free carbon bonds. Therefore, most of the processes can be completed at room or mild temperature with simpler procedures and more kinds of functional groups or heteroatoms can be implanted.

In addition to sulfur infiltration, sulfur/GO configuration, and physical/chemical interaction, other factors such as electrolyte solvent [153], electrolyte additive concentration [154], operating temperature [114], and graphene alignment [155] may affect the performance of GO-based electrodes. The vertically aligned sulfur-graphene (S-G) nanowalls simultaneously facilitated electron/ ion transfer and buffered volume change, enabling a high capacity of 410 mAh/g at 8 C rate [155]. The flexible nature of GO is attractive in fabricating flexible electrodes [33,156,157]. Zinc foil was used to reduce GO and load sulfur nano particles (SNP) in between rGO sheets via a chemical method. The obtained rGO/SNP paper exhibited superior mechanical properties (a tensile strength of 68 MPa and Young's modulus of 965 MPa) and electrochemical performance (500 cycles at 1 C rate) [33]. A cold-quenching and freeze drying method was employed to fabricate rGO nanotube wrapped sulfur nanoparticles (RGONT@S). The RGONT@Scomposite film showed a tensile strength of 18.1 MPa and a Young's modulus of 1.2 GPa [157]. In the aforementioned two studies, soft batteries were assembled and tested under bending/twisting conditions, which validated the feasibility and mechanical robustness of GO based flexible batteries.

Although GO is tunable in terms of composition and configuration, it is still beyond a perfect sulfur carrier. The drawback of GO is its relatively low conductivity comparing with graphene and other carbon materials which have intact crystal structures, often resulting in a poor electrochemical performance at high current density regimes. For instance, when sulfur is incorporated with pure GO or rGO, the highest current density which can delivery stable discharge capacity rarely exceeds 5 C (see Table S1 in Supplementary data). Moreover, GO and rGO often exhibit poor mechanical properties because they contain a large amount of defects, which deteriorates the cyclic ability. Apart from the technical challenges, the current fabrication methods of GO is not costefficient and environmentally benign. Low-cost, scalable processes are required for industrial production and commercialization of GO related products.

5.3. Graphene/GO/rGO based composites for Li-S batteries

As discussed in the previous two sections, both graphene and GO/rGO scaffolds have intrinsic shortcomings which are difficult to overcome by simply changing sulfur infiltration methods and/or graphene/sulfur configurations. The unparalleled advantage of graphene and its derivatives is their exceptional compatibility with other materials, including carbon materials, polymers, and metal compounds, offering many rational design routes to overcome the intrinsic shortcomings such as compositing graphene with polysulfide immobilizing materials or compositing GO/rGO with highly conductive materials.

Because of the abundance and diversity, carbonaceous materials are widely incorporated with graphene/GO/rGO to enhance

the ion/electron conductivity and/or polysulfide entrapping ability. As a kind of carbon material with special 1D morphology and outstanding conductivity, carbon nanotubes (CNTs) have been employed in different applications [158-160]. CNT reinforced graphene/GO composites largely improved the performance of Li—S batteries. The production routes of CNT reinforced graphene/ GO composites can be grouped into two categories: direct mixing and in situ growth. The first approach is to mix CNTs with graphene [161], rGO [87,88,162–168], or functionalized GO [169]. A leaf-like GO scaffold with CNT midribs was synthesized by compositing CNTs with GO in the middle process stage of Hummer's method. The assembled batteries exhibited an outstanding lifespan of 500 cycles with only 0.081% capacity decay per cycle even at a high sulfur content of 85% [168]. Cetyltrimethylammonium bromide modified GO was combined with CNTs to construct a porous, conductive scaffold. The assembled battery exhibited a high energy density of 332 Wh/kg with high sulfur loading (11.5 mg/cm²) and low electrolyte/sulfur (E/S) ratio (4) [169]. The second approach is to grow CNTs in situ on graphene matrix by using Co [88], Ni [170], Fe/Co [171], Fe/Mo [172], Ni/Co [173], or FeMgAl LDH [174] catalysts. Cobalt was employed as the catalyst and urea acted as the carbon source in a one-pot pyrolysis process to synthesize 3D graphene nanosheet-carbon nanotube (GN-CNT) scaffold. Such 3D GN-CNT scaffold rendered outstanding ionic/electric conductivity and the interactions of cobalt nanoparticles and N/O heteroatoms with polysulfides. Armed with such syngeneic enhancements, the battery exhibited eminent stability [88]. In addition to the enhancement of electrochemical performance. CNTs also improved the mechanical robustness of the graphenebased scaffolds, which is essential for the fabrication of flexible devices. A robust carbon nanotube-rGO/sulfur (CNT-rGO/S) composite exhibited a tensile strength of 62.3 MPa even after 120 cycles [167].

Another interesting approach is to composite graphene with GO, compensating each other's disadvantages. GO aerogel was infiltrated into graphene foam (GF) with interconnected networks fabricated by depositing carbon on nickel foam via CVD method, forming a GF/rGO scaffold. The GF/rGO scaffold exhibited an outstanding conductivity from graphene, a highly porous structure from rGO aerogel, and an eminent sulfur entrapment ability from functional groups, making it a superlative sulfur carrier with an ultrahigh sulfur loading of 9.8 mg/cm² and a stable reversibility as of 350 cycles [38]. In another route, a conformal multilayered graphene coating was recently deposited on the GO/Li₂S nanospheres to form the core-shell structure for Li₂S/GO@C cathode. The graphene coating entrapped polysulfides and enhanced conductivity. The assembled battery exhibited a long lifespan of 1500 cycles and an outstanding rate ability of 269 mAh/g at 6 C [109]. Ke Chen et al. in situ grew nitrogen-doped graphene-like porous carbon on GO substrate via MOF templates. Such sulfur carrier enabled ultra-low capacity decay per cycle [175]. Graphene, GO, and CNTs have been integrated to form a rGO/CNT scaffold with a graphene shell, which immobilized polysulfides and minimized the irreversible capacity loss and self-charging [176].

Another conductive carbon material which was composited with graphene/GO is hollow carbon nanospheres or nanocages [177–180]. The hollow structure offered physical confinement for sulfur and polysulfides while the graphene coating cemented layers of spheres/cages, facilitating the electronic/ionic transfer. A layer-by-layer (LBL) self-assembly strategy was explored to fabricate functionalized graphene/polyelectrolyte multilayer (PEM) hollow carbon spheres/sulfur composite. The strong electrostatic interactions between the oppositely charged materials made the coating agents stable and the coating procedure highly efficient [178].

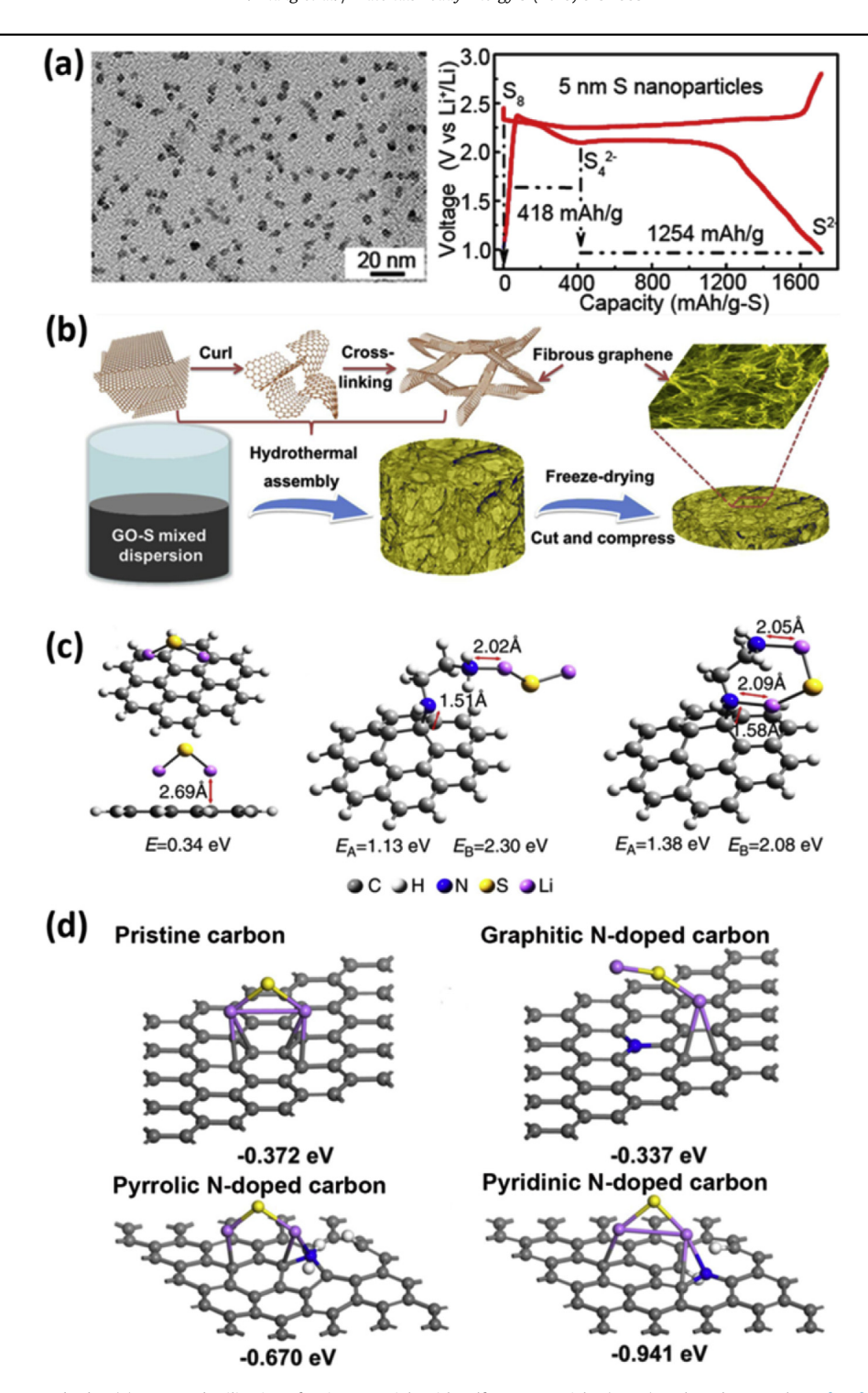


Fig. 4. GO/rGO for Li–S battery cathodes. (a) Improved utilization of active materials with sulfur nanoparticles (5 nm) anchored on GO sheets [105]. (b) Fabrication procedures of 3-D GO sponges with interconnected pores [36]. (c) DFT simulation of Li₂S interacting with EDA functional groups, showing much higher bonding energy than pristine graphene [84]. (d) DFT calculations of the interactions between sulfur and nitrogen atoms, showing that pyridinic N atoms have the strongest interaction with polysulfides. Images reproduced from Refs. [36,84,105,143].

Cost is an important issue that must be considered in cathode fabrication. Graphene, GO, and CNT are not low-cost material at the current stage; therefore it is a worthy topic how to minimize the graphene/GO consumption while maximizing the function. Activated carbon, which is relatively low-cost yet sufficiently porous, is a good option to balance the cost and performance. Nanoporous activated carbon is able to encapsulate polysulfides and promote

the stability of Li—S batteries [32,181—185]. A hierarchically porous carbon scaffold consisting of graphene, mesoporous carbon, and super P with a glass-fiber membrane enabled an ultra-high sulfur loading of 13 mg/cm² and a high areal capacity of 14.3 mAh/cm² [184]. A two-dimensional (2D) carbon yolk-shell nanostructure: graphene encapsulated in hollow mesoporous carbon nanosheet (G@HMCN), exhibited a balance between the areal (5.7 mAh cm⁻²)

and volumetric (1330 mAh cm⁻³) capacities [185]. Graphene, CNT, and nanostructured porous carbon were combined and the highly conductive network enabled outstanding rate capability [186].

Recently, bio-mass derived activated carbon materials have attracted much attention due to their naturally porous structure and abundant raw material resources [34,187,188]. Our group has devoted to developing low-cost, high-performance Li-S batteries by combining graphene with porous carbon scaffold derived from bio-mass materials. A conductive activated cotton textile (ACT) with porous tubular structure was derived from natural cotton textile [146]. The flexible carbon scaffold was then loaded with sulfur and wrapped with partially rGO, forming ACT/S-rGO composite (Fig. 5a). The rGO layer not only immobilized lithium polysulfides, but also served as a conductive coating, which mitigated the poor conductivity of sulfur and enabled fast electron transportation along ACT fibers. The assembled ACT/S-rGO cathode with porous ACT interlayer exhibited an exceptional rate capability and durable cyclic performance (with a well-retained capacity of 1016 mAh/g even after 200 cycles). A flexible Li-S cell with ACT/SrGO as a cathode was also assembled to demonstrate its superior potential as flexible power sources for future wearable electronic devices. In another design, recycled paper fibers were wrapped with graphene sheets via a capillary adsorption method, remarkably improving sulfur loading and cathode conductivity (Fig. 5b) [95]. The graphene/activated paper carbon (APC) scaffolds enabled superior lifespan of 620 cycles with an excellent capacity retention rate of 60.5%. Instead of compositing graphene/GO with solely activated carbon, we also explored the possibility of combining two other distinctive materials with graphene/GO in Li-S batteries. Orderly arranged nanopores with unique Ni/graphene core/shell nanoparticles were decorated on the activated banana peel (ABP) by annealing the Ni(NO₃)₂ solution-treated banana peel pieces [74]. Ni(NO₃)₂ decomposed into Ni nanoparticles and HNO₃ during heating. The corrosive HNO3 vapors etched the ABP surface, creating a nanoporous structure with an average pore size of 30 nm. At high temperature, the carbon atoms from ABP dissolved into Ni. When the sample cooled down to room temperature, the carbon atoms precipitated out and segregated on the Ni nanoparticle surface, forming multilayered graphene shell (Fig. 5c). The Li-S batteries built by the ABP/Ni/graphene hybrid achieved exceptionally high electrochemical properties in terms of specific capacitance (1260.3 mAh/g at 0.2 C), rate capability, and cycling robustness.

Another alternative strategy is to composite graphene/GO with conductive polymers, which not only physically encapsulate dissolved polysulfides, but also buffer the volume fluctuation, preventing cathodes from pulverization. Some polymers may enhance the conductivity or chemical interactions with sulfur/polysulfides. Polyethylene glycol (PEG) was found to be able to wrap sulfur particles, encapsulating polysulfides and buffering the volume change [98,189]. Amylopectin [190], polydimethylsiloxane (PDMS) [73], polydopamine (PDA) [191], polyvinylpyrrolidone (PVP) [192,193], polypyrrole (PPy) [194], and poly (3,4-ethylene-diox ythiophene):poly(styrenesulfonate) (PEDOT:PSS) (SGP) [195] exhibited similar functions. Polyacrylonitrile (PAN) constructed rigid scaffolds rendered higher sulfur loading and energy density [26,196,197]. Polydiallyldimethylammonium chloride (PDDA) was found to positively charge the graphene/sulfur composite, leading to a strong electrostatic interaction with polysulfides [198]. Poly(anthraquinonyl sulfide) (PAQS), on the other hand, tends to interact intensively with polysulfides, increasing ionic conductivity and thus resulting in a long lifespan of 1000 cycles and a remarkable capacity retention rate of 61.5% when the current density was increased from 0.25 C to 8 C. Impressively, at 8 C rate, the battery still delivered a specific capacity of 615 mA h/g [112]. A copolymerized aniline and phytic acid (PA) on GO framework, on the other hand, utilized the strong interaction between quinonoid imine functional groups and polysulfides, leading to a high areal specific capacity [199].

It has been proven that metal oxides often exhibit strong absorption ability to different ions and molecules [200-202]. Therefore, metal oxides, metal nitrides, metal carbides, or metal sulfides have been composited with graphene/GO/rGO, making such configurations promising for high-performance Li-S batteries [21,80,89,115,203-210]. A TiO₂ layer was deposited on nitrogen doped graphene-sulfur hybrid (NG-S) by atomic layer deposition (ALD). The strong interaction between polysulfides and TiO₂ effectively mitigated the shuttle effect [89]. Similarly, ZnO and MgO layers were separately coated on the rGO/S composite to prohibit the dissolution and migration of polysulfides, leading to an outstanding capacity retention (89% after 100 cycles) [115]. Another interesting process is to reduce KMnO₄ to MnO₂ by sulfur, forming a honeycomb-like MnO2 shell, which produced abundant voids for storing polysulfides. The outermost GO coating was assembled to block the open pores of MnO₂, improving the conductivity of the electrode [206]. An alternately stacking graphene and layered graphitic C₃N₄ with a cross-linked elastomeric binder framework achieved an ultra-high sulfur loading of 14.9 mg/cm² and low electrolyte/sulfur ratio of 3.5: 1 μL mg⁻¹ [207]. A hydrothermal method was employed to fabricate vanadium nitride/graphene (VN-G) composite. When being used as electrodes, VN strongly bonded with polysulfides and largely improved the conductivity, achieving an outstanding capacity retention and rate ability [208]. TiC was composited with graphene and proven the crucial role of the conductivity of the polar host in the electrochemical kinetics of Li-S batteries [209]. Iodine doped GO/NbS2 cathode exhibited an outstanding performance - 2000 cycles at 40 C rate [80]. GO and NbS2 were found to intensively interacted with dissolved polysulfides. Moreover, active sulfur species often intercalated in the interlayers of NbS₂, further enhancing the intrinsic conductivity and polarity. Even when the sulfur loading was increased up to 3.25 mg/ cm², the battery still achieved 600 cycles at 1 C rate [80]. Unlike most of the studies, CoS₂ in rGO/CoS₂ cathode was found to enhance liquid-liquid redox of polysulfides by forming high-efficient charge-transfer junctions, which ignited the whole solid-liquidsolid electrochemistry of sulfur in an aprotic electrolyte [210]. The finding suggests that the surface redox in Li-S battery is critical but has not been comprehensively understood.

5.4. Beyond cathode

Instead of cathode, graphene, GO/rGO, and their composites have been exploited in other components of Li-S batteries. To improve sulfur utilization and eliminate shuttle effect, a bifunctional cathode interlaver was put forward in the Li-S battery system [211,212]. A qualified cathode interlayer should be lightweight, robust, flexible and have a strong interaction with polysulfides, which are typical features of graphene and its derivatives. rGO was first used to build cathode interlayers, rendering high specific capacity and cyclic ability (Fig. 6a) [113,213]. Oxides, sulfides, and nitrides, such as TiO₂ [214], MnO₂ [215], MoS₂ [216], and BN [217], have been composited with graphene for the cathode interlayers. Because of the strong interaction between metal oxides and polysulfides, the battery with TiO₂/graphene interlayer showed a low capacity degradation rate of 0.01% and 0.018% per cycle, measured over 1000 cycles at 2 and 3 C, respectively [214]. A prototype supramolecular material, cucurbituril (CB), was then integrated with graphene, forming an interlayer. As an efficient lithium polysulfides capsule for Li-S batteries, CB has a large atomic fraction of binding sites, effectively reducing shuttle effect [218]. The

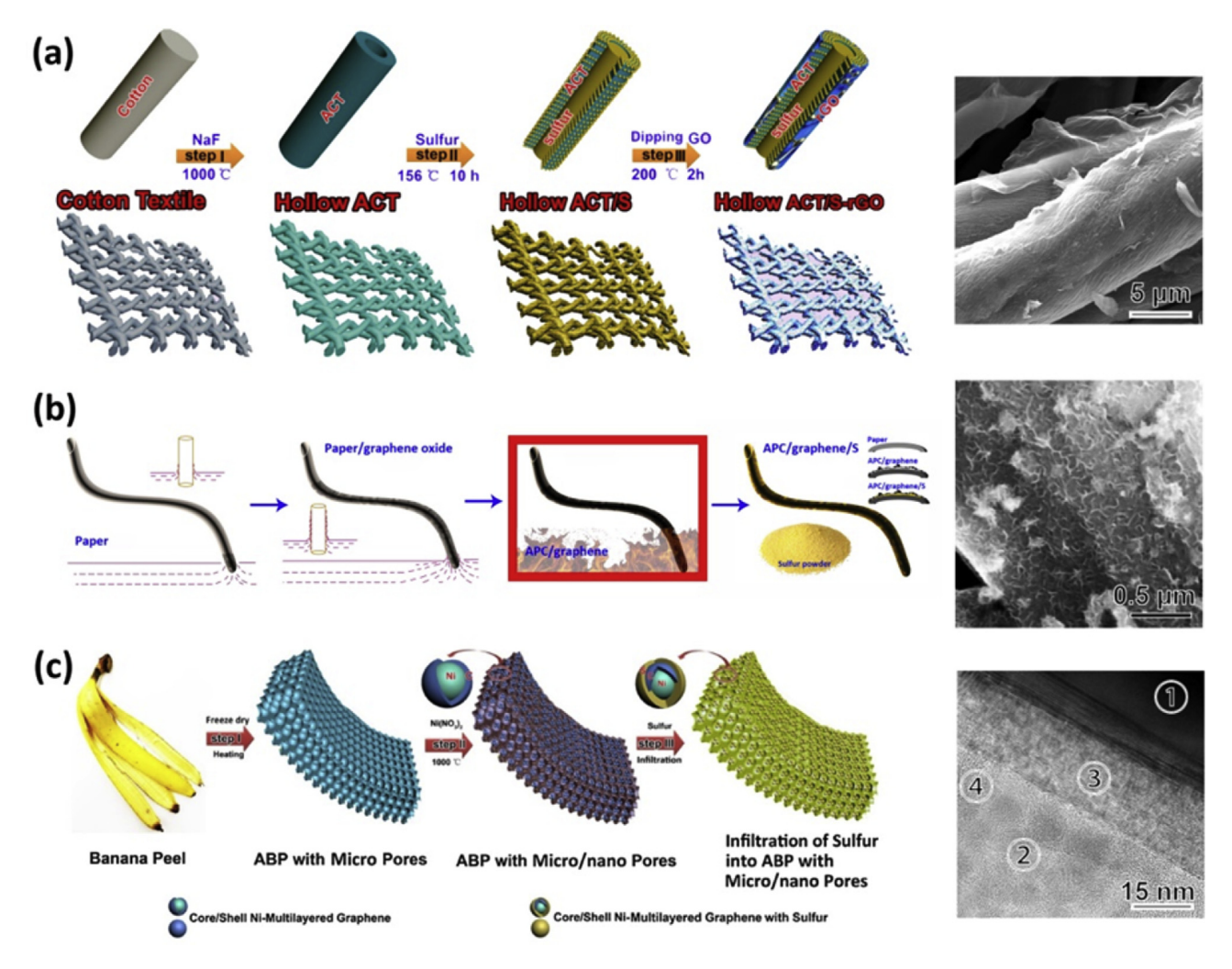


Fig. 5. Graphene/GO/bio-mass derived carbon hybrid materials. (a) ACT fibers wrapped with rGO. The ACT offered superior conductivity and flexibility [146]. (b) APC fibers wrapped with GO via capillary absorption. In the following heating, GO contracted, forming tortuous nano budges, which encapsulated sulfur and enhanced electron transfer [95]. (c) Graphene precipitated on the Ni nanoparticles on ABP surfaces. The graphene/Ni core/shell structure increased conductivity and specific surface area, leading to a better performance of the assembled battery [74]. Images reproduced from Refs. [74,95,146].

interlayer, however, was a "dead weight" for the battery since it did not participate in the chemical reactions. Therefore, it is critical to reducing the volume fraction of the interlayer component. An ultrathin interlayer with less than 100 nm in thickness and <1% in volume compared with the cathode was recently synthesized by mixing naphthalimide-functionalized poly(amidoamine) (PAMAM) G4 dendrimer (Naph-Den) and mildly oxidized graphene oxide (mGO). The amide-containing dendrimer molecules interacted actively with polysulfides, leading to an outstanding capacity retention rate (0.008% capacity decay per cycle) [219].

The separator is a critical component of a battery system. A superior separator for Li–S batteries should not only have a good ionic conductivity, but also suppress the migration of polysulfides during cycling. Since traditional separators are unable to meet such requirements, new separators fabricated by graphene composites have been developed [90,220–228]. When being used as a separator, GO exhibited a permselective mechanism. The oxygen electronegative atoms modified GO to a polar plane, which allowed the transition of positively charged species (Li⁺) while rejecting the transportation of negatively charged species (S_n²) due to the electrostatic interactions [220]. To further promote such mechanism, Li₄Ti₅O₁₂ (LTO) [223] and MOF [90] were separately composited with rGO via vacuum-filtration. The LTO nanospheres had a high

chemical affinity with polysulfides and an excellent ionic conductivity; the MOF particles endowed a feasible ion transfer pathway while blocking the dissolute polysulfides; the graphene layers cemented the particles, serving as a physical barrier for polysulfides. Batteries with the LTO/rGO or MOF/rGO separators exhibited ultralow capacity decay rate. A twinborn TiO2—TiN heterostructure was recently composited with GO for Li—S battery separators. The merits of highly adsorptive TiO2 with conducting TiN was well combined and achieved smooth trapping—diffusion—conversion of lithium polysulfides across the interface [227].

Graphene and its derivatives also have the potential to be used in current collectors, electrolytes, and anodes. A graphene constructed current collector enabled outstanding lifespan and rate ability because it was able to entrap polysulfides and improve the battery conductivity (Fig. 6b) [229]. The rGO electrolyte additives have been proven to enhance ionic and electronic conductivities while reducing the lithium ion diffusion length and buffering the stress/strain in all-solid batteries, promoting the cyclic stability and lifespan [118,230]. Graphene/GO was found to stabilize Li anode [231]. The anode constructed with graphene wrapped Li_xM (M = Si, Sn, or Al) nanoparticles exhibited an outstanding resistance to air and water (Fig. 6c). When coupling with sulfur as the cathode, the

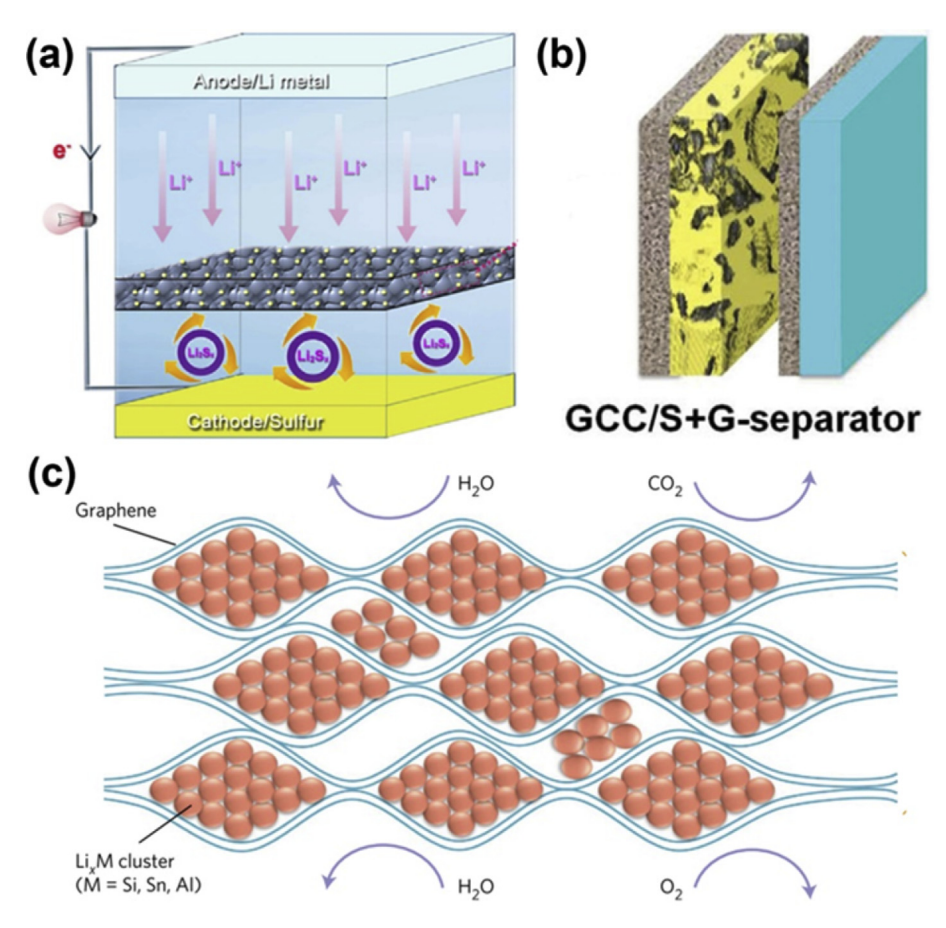


Fig. 6. Graphene and its derivatives for battery components other than cathode. (a) Graphene/carbon black cathode interlayer anchored on polysulfides [213]. (b) Graphene as both current collector and cathode interlayer [229]. (c) Graphene wrapped Li_xM (M = Si, Sn, or Al) nanoparticle anode, showing an outstanding resistance to air and water [231]. Images reproduced from Refs. [213,229,231].

full cell demonstrated an excellent cycling stability at 0.5 C and maintained a capacity of 858 mA h/g after 110 cycles with a coulombic efficiency of 99.5% [231]. The SEI-coated graphene (SCG) framework, on the other hand, effectively prevented the growth of dendrites [232].

6. Reflection and prospection

Clearly, graphene and its derivatives have been widely used in Li-S system and largely enhanced Li-S battery performance. Fig. 7a shows the publications on graphene/Li-S batteries from 2011 to 2017. With the discovery of graphene [39,40] and the conceptproving study showing that sulfur/porous carbon largely improved the battery stability [32], publications on grapheneenabled, high-performance Li-S batteries experienced a rapid growth since 2011 and reached a peak at 2015. Subsequently, publications slowed down in 2016 because sulfur infiltration methods and graphene/sulfur configurations were comprehensively studied. Efforts on seeking a joint improvement of battery performance [21] and high sulfur loading cathode [233] have pushed up research activities. Based on the publications listed by categories (Fig. 7b), studies on scaffolds with GO/rGO and graphene reached the peak in 2014 and 2015. The development of graphene/ GO based composites followed up rapidly. In the year of 2017, more than half of the publications are related to composites indicating that graphene/GO based composites are promising for highperformance Li-S batteries.

Table S1 in the Supplementary data summarizes the electrochemical properties of assembled whole Li–S batteries. The corresponding statistical cartograms are plotted in Fig. 8. A parameter which reflects the maximum utilization of sulfur is the discharge capacity at the first cycle. Intriguingly, the average number has not been changed much from 2011 to 2017; it stabilized between 1150 and 1250 mA h/g_{sulfur}, representing a 65-75% utilization of sulfur (Fig. 8a). The stable initial discharge capacity, on one hand, validates that graphene containing scaffolds effectively overcome the insulating nature of sulfur even in simple mixing scenarios; on the other hand, the stagnation of improvement suggests that the irreversible loss of active materials has not been effectively eliminated even though numerous methods were attempted. Unlike the initial discharge capacity, the average lifespan of Li-S batteries with graphene/GO cathodes improved chronologically from 2011 to 2015, and achieved 500 stable cycles since then (Fig. 8b). Such long lifespan results from the synergic effect from the electrodes and electrolyte. The advanced configuration between sulfur and graphene (Table 2) enabled the cathode to buffer the large volume fluctuation during discharging/charging and mitigated the degradation of both cathode and anode. Electrolyte additives, especially LiNO₃ [234,235], were found to form a protective layer on the Li anode, largely enhancing the stability. The capacity decay per cycle also decreased year by year and the average number stabilized at about 0.1% in the recent three years (Fig. 8c). Such improvement mainly stems from an increasing understanding of the fundamental reaction mechanisms of Li-S system. Materials with stronger interactions with polysulfides, such as heteroatoms, functional groups, metal oxides, and metal nanoparticles, were integrated with graphene/GO/rGO to achieve a better polysulfide immobilizing ability. Another critical property of

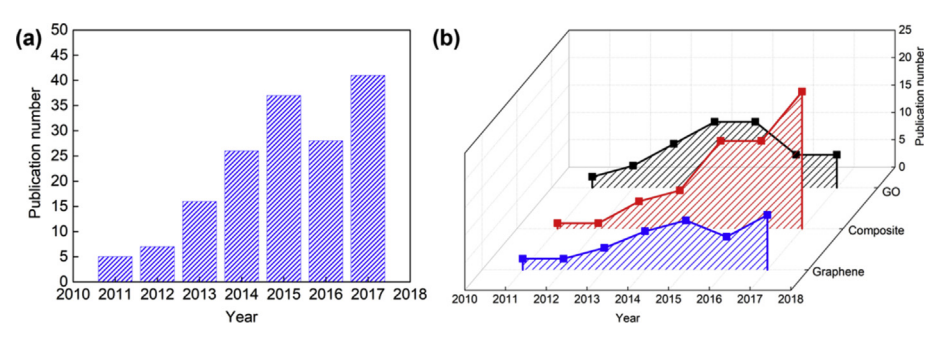


Fig. 7. Statistical results of publications on graphene/GO for Li—S batteries (based on the online published date). (a) Publications reached a peak in 2015 and slowed down in 2016 but bounced back in 2017. (b) Publications on graphene/GO based cathodes reached a peak at 2014. More studies followed up rapidly on composites after 2015, indicating that graphene/GO based composites are promising for high-performance Li—S batteries.

Li—S battery is the rate capability. It is difficult to normalize this property because different current density regimes or even different units were employed to characterize the rate performance (Table S1). The rate capability has a noticeable improvement since 2011 in terms of capacity retention at higher current density regimes and the highest current density that the battery can tolerate. The enhancement of rate capability resulted from improved electron/ion transfer capacity due to the formation of sulfur nanodomains and the assistance with highly conductive materials (graphene), which enhanced the kinetics of S₈ dissolution and Li₂S formation, respectively.

Three critical properties – lifespan, capacity retention, and rate ability – have been notably improved after the employment of graphene and its derivatives in Li-S batteries. In fact, in the year of 2015, the most advanced Li-S batteries with graphene-based scaffolds operated over 1000 cycles with a stable energy output at over 5 C current density with a capacity decay lower than 0.1%. Such eminent performance is comparable to or even better than commercialized Li-ion batteries. An interesting question arises: why are Li-S batteries still at a conceptual level? If we reexamine the cartograms, except for the relative constant initial discharge capacity (Fig. 8a), both the lifespan (Fig. 8b) and capacity decay rate (Fig. 8c) have barely improved after 2015, which is the year when the number of publications reached the first peak (Fig. 7a). The question, together with the stagnated improvement after 2015, reflects an undoubted fact that the development of Li-S batteries is encountering a bottleneck. Standing on the brink of next breakthrough, it is urgent for the community to rethink the ground challenges.

Energy density, both gravimetric and volumetric, is one of the major roadblocks on the way to commercializing Li—S batteries. Although the theoretical energy density of Li—S battery is 2600 Wh/kg, the assembled Li—S batteries seldom achieve an

energy density over 300 Wh/kg. The following three major challenges severely hamper the improvement of energy density. The first one is the amount of sulfur in the cathode. Two variables are often used to characterize the amount of sulfur: sulfur content and sulfur loading (Fig. 9). Sulfur content indicates the weight percentage of sulfur in the cathode; sulfur loading means the areal weight of sulfur with the unit of mg/cm². These two parameters, although correlated, are not linearly dependent. Current cathodes are often with low sulfur content (lower than 70%) and low sulfur loading (lower than 5 mg/cm²). The low concentration of sulfur benefits the utilization of active materials and reduces the degradation of electrodes, rendering a deceptive long lifespan and high specific capacity. A thick and porous cathode with high sulfur loading but low sulfur content requires extra electrolyte to wet the cathode, which inevitably decreases the energy density. The high sulfur content configuration weakens the electronic/ionic conductivity, constraining electrode thickness and leading to poor rate performance. Thus, it is difficult to simultaneously achieve high sulfur loading and sulfur content (Fig. 9).

The second challenge is the sulfur utilization. As shown in Fig. 8a, the average initial discharge capacity often falls in the range between 1150 and 1250 mA h/g, indicative of a 65–75% of sulfur utilization. It is anticipated that 90% sulfur utilization should yield a specific capacity of 1500 mA h/g and 20% amplification in the energy density. A Li–S battery with sulfur-nanoparticle/GO constructed cathode displayed an initial discharge capacity of 1672 mA h/g [105]. Recently, a low-surface-area, open carbon fiber architecture was used to control the nucleation and growth of sulfur species by manipulating the carbon surface chemistry and the solvent properties, leading to ~100% sulfur utilization over 100 cycles [236]. Intriguingly, the high sulfur utilization of these two configurations all derived from surface reactions, not from the physical encapsulation from porous structures, implying that the

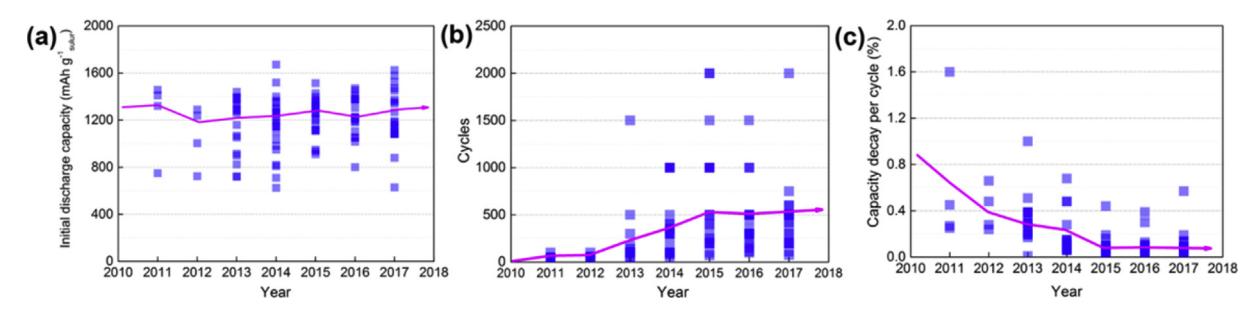


Fig. 8. Statistical data of the electrochemical properties of Li–S batteries with graphene. (a) The discharge capacity at the first cycle, showing no obvious change from the year 2011 to 2017. (b) The lifespan of Li–S batteries with graphene based cathodes increased constantly from 2011 to 2015 and stabilized in the recent three years. (c) The capacity decay per cycle decreased from the year 2011 to 2015 and stabilized at about 0.1%.

commonly held belief that sulfur needs to be wrapped by conductive substrate requires to be re-thought; more fundamental studies on the interfacial reaction mechanisms are demanded.

The last challenge is the amount of electrolyte. According to a recent calculation [169], when the electrolyte/sulfur (E/S) ratio reaches 10, it is impossible to achieve an energy density of 300 Wh/kg no matter how high the sulfur loading is. If the E/S ratio is decreased down to 5, an energy density of 300 Wh/kg can be achieved with about 75% sulfur utilization and 10 mg/cm² sulfur loading. For the goal of 500 Wh/kg, it is suggested that the E/S ratio needs to be lower than 3, and sulfur utilization of 80% and sulfur loading of 10 mg/cm². The most difficulty in reducing the amount of electrolyte is how to sustain the ionic conductivity while preventing the continued consumption of additives. Therefore, it is critical to find low-cost, high-performance electrolyte additives or to develop reliable solid-state electrolytes.

Another roadblock to the commercialization of Li—S batteries is the Li anode. For practical application, safety and stability are both on the top of priority. Metal Li is highly active when being exposed to air or water, bringing safety risks and increasing transportation and assembling cost. When coupled with sulfur-containing cathodes and organic electrolytes, Li anodes are inevitably obsessed by uncontrolled side reactions. Large dendrites often form during charging, penetrating the separator and leading to "sudden death" or even thermal runaway [237]. Li whiskers, which are also called mossy Li, were found to grow inhomogeneously on Li surface, promoting the formation of passive sediments and consuming electrolyte [238]. The employment of Li₂S₈ additive [239] or glass fiber film anode interlayer [240] suggested stronger spontaneous or artificial solid-electrolyte interface (SEI) can effectively mitigate the side reactions.

Thusly, the development of Li—S batteries is at a crossroad. Fortunately, graphene and its derivatives render the confidence that the bottlenecks will be broken by the rational designs of graphene and/or its derivative based sulfur/lithium composites. Previous studies have displayed possible solutions for the aforementioned challenges. A graphene/sulfur composite fabricated by a reverse (water-in-oil) microemulsion technique achieved a 94% sulfur content and 8 mg/cm² sulfur loading [81]. An S-GO-CTA-CNT nanocomposite prepared by freeze drying method gained 75%

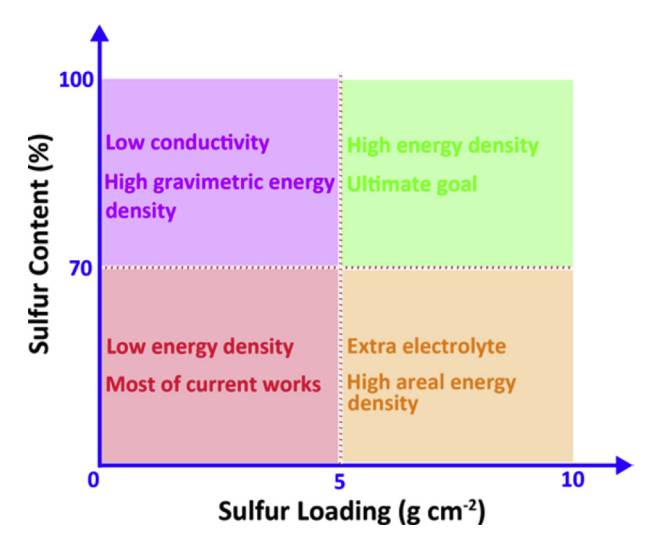


Fig. 9. Relationship between sulfur content and sulfur loading. Most of the studies employed graphene scaffolds with low sulfur content and low sulfur loading. A thick and porous cathode with high sulfur loading but low sulfur content requires extra electrolyte to wet the cathode, which inevitably decreases the energy density. The high sulfur content configuration weakens the electronic/ionic conductivity, constraining electrode thickness and leading to poor rate performance.

sulfur content and 11.1 mg/cm² sulfur loading [169]. The two studies suggest that homogeneously mixing mono or few-layered graphene with sulfur is the key to simultaneously accomplish high sulfur loading and high sulfur content. When nano-sized sulfur particles homogeneously dispersed on GO or functionalized graphene sheets, the small particle size enables fast electron exchange and the attached functional groups/heteroatoms can bond with polysulfides, effectively reducing the irreversible dissolution. Together with physical confinement, graphene based cathodes can achieve high sulfur utilization [105,195]. The GO additive demonstrated in Ref. [230] proven graphene is able to enhance the ion transfer in the solid electrolyte, indicating that graphene/GO may be used as conductivity reinforcer in electrolytes. A promising solution for the Li anode issues is to wrap Li with graphene, shielding Li [231]. Considering the strength and flexibility, graphene has great potential to be an artificial SEI for lithium anode without adding much extra weight to the cell. This postulation was preliminarily verified by the graphene wrapped Li anode [231], in which no dendrites formed on the electrode surface. Therefore, graphene and its derivatives, on the cathode side, are able to encapsulate sulfur particles, bond with polysulfides, and enhance electronic/ionic conductivity; on the anode side, they can stabilize Li metal and eliminate side reactions.

Although previous studies have depicted a promising solution of overcoming the Li-S battery challenges, graphene and its derivatives also have their disadvantages. Scientifically, the conductivity of graphene is often compromised by the number of functional groups and heteroatoms, which are critical for the polvsulfide immobilization. Therefore, it is difficult to achieve simultaneously high conductivity and high polysulfides adsorption by sole graphene frameworks. Besides, the bonding energy between polysulfides and functionalized/doped graphene is still weaker than that between polysulfides and metal oxides, metal nitrides, or metal sulfides. Practically, graphene and GO are not cost-efficiency materials at the current stage considering the time and material expanse. Moreover, graphene sheets tend to aggregate so require special storage and transportation methods. In order to fabricate practical graphene based Li-S battery products and accelerate their commercialization, in addition to a scale-up, low-cost graphene production method, there are three directions which need further development:

- 1) Deeply understand the interactions between graphene, functional groups, heteroatoms and sulfur, polysulfides. Although several studies have focused on the interactions and made notable progress, but it is far beyond a comprehensive understanding, especially at quantitative level. If quantitative and statistic conclusions are obtained from theoretical and experimental results, we can optimize the amount of functional groups/heteroatoms and sulfur/carbon ratio, largely improving the utilization efficiency of sulfur and graphene;
- 2) Explore high-performance, low-cost graphene composites. Graphene based composites for Li—S battery cathodes have shown unparalleled advantages comparing with sole graphene frameworks. However, most of current studies on the composites are based on trial-and-error experiences without a systemic principle. Advanced computational methods, such as machine learning, probably can help us to find the best recipe.
- 3) Expand applications of graphene and its derivatives to separator, binder, electrolyte, and anode. Unlike extensive studies on the cathodes, applications of graphene and its derivatives on other parts of Li—S batteries are underdeveloped. Achieving outstanding performances requires a holistic improvement of every part and graphene has great potential for enhancing separator, binder, electrolyte, and anode.

7. Summary

Graphene and its derivatives have been widely utilized in Li-S batteries and effectively enhanced their electrochemical performance because of their outstanding mechanical strength, exceptional conductivity, and large specific area which can buffer the large volume change, suppress the insulating nature of sulfur, and physically encapsulate sulfur particles. A strong van der Waals' interaction occurs between graphene and sulfur, endowing outstanding wettability and facilitating various sulfur infiltration methods and sulfur/graphene configurations. Functional groups on GO sheets have been proven to have a strong interaction with lithium polysulfides, effectively reducing the shuttle effect and improving the utilization of active material. The physical and chemical interactions of graphene and GO with sulfur/polysulfides can be further enhanced via multiple approaches, such as constructing porous architecture, functionalizing, and doping. Compositing graphene/GO with other materials has become a more efficient and effective approach for low-cost, high-performance Li—S batteries. In addition to cathodes, graphene and its derivatives were used as interlayers or separators to impede the migration of dissolved polysulfides, thereby reduce the shuttle effect. GO were also employed as the conductivity reinforcer in solid electrolytes. Recently, it was found that graphene in Li anodes was able to prevent the Li dendrites growth and the spontaneous degradation. The development of Li-S battery technology is currently at a crossroad. The low energy density due to low sulfur loading, high electrolyte dosage, and low sulfur utilization, as well as the safe and cost issues from Li anode, hinder the scale-up production and commercialization of Li-S products. Graphene and its derivatives are promising to game-change Li-S batteries.

Acknowledgements

The authors acknowledge the financial support provided by the U.S. National Science Foundation (CMMI-1728042, CMMI-1418696, and CMMI-1358673) and the i6 Virginia Innovation Partnership.

Appendix A. Supplementary data

Supplementary data related to this article can be found at https://doi.org/10.1016/j.mtener.2018.06.001.

References

- [1] C. McGlade, P. Ekins, Nature 517 (2014) 187-190.
- [2] S. Chu, Y. Cui, N. Liu, Nat. Mater. 16 (2017) 16-22.
- [3] R.Q. Ã, S. Peterson, Energy Policy 35 (2007) 5938-5952.
- [4] S. Brown, D. Pyke, P. Steenhof, Energy Policy 38 (2010) 3797–3806.
- [5] Tesla Model S Charging Estimator. https://www.tesla.com/models.
- [6] R. Van Noorden, Nature 507 (2014) 26–28.
- [7] M.F. Rodrigues, et al., Nat. Energy 2 (2017) 17108.
 [8] X. Wang, et al., Adv. Mater. 26 (2014) 4763–4782.
- [9] A. Yoshino, Angew. Chem. Int. Ed. 51 (2012) 5798-5800.
- [10] J.B. Goodenough, Y. Kim, J. Power Sources 196 (2011) 6688–6694.
- [11] J.B. Goodenough, Y. Kim, Chem. Mater. 22 (2010) 587-603.
- [12] V. Etacheri, et al., Energy Environ. Sci. 4 (2011) 3243-3262.
- [13] B. Dunn, et al., Science 334 (2011) 928–935.
- [14] M.M. Thackeray, et al., Energy Environ. Sci. 5 (2012) 7854.
- [15] L. Lu, et al., J. Power Sources 226 (2013) 272-288.
- [16] L. Cui, et al., Nano Lett. 9 (2009) 3370-3374.
- [17] G. Derrien, et al., Adv. Mater. 19 (2007) 2336–2340.
- [18] P. Poizot, et al., Nature 407 (2000) 496-499.
- [19] S.S. Zhang, J. Power Sources 162 (2006) 1379–1394.
- [20] P.G. Bruce, et al., Nat. Mater. 11 (2011) 19-29.
- [21] Q. Pang, et al., Nat. Energy 1 (2016) 16132.
- [22] S. Urbonaite, T. Poux, P. Novák, Adv. Energy Mater. 5 (2015) 1500118.
- [23] S.E. Cheon, et al., J. Electrochem. Soc. 150 (2003) A796-A799. [24] S.E. Cheon, et al., J. Electrochem. Soc. 150 (2003) A800-A805.
- M. Wild, et al., Energy Environ. Sci. 8 (2015) 3477-3494.
- [26] Z. Li, et al., Nat. Commun. 6 (2015) 8850.

- [27] D. Lin, Y. Liu, Y. Cui, Nat. Nanotechnol. 12 (2017) 194-206.
- [28] P.P.R.M.L. Harks, et al., Adv. Energy Mater. 7 (2017) 1601635.
- [29] Y.V. Mikhaylik, J.R. Akridge, J. Electrochem. Soc. 151 (2004) A1969-A1976.
- [30] A. Manthiram, S.H. Chung, C. Zu, Adv. Mater. 27 (2015) 1980–2006.
- [31] M.A. Pope, I.A. Aksay, Adv. Energy Mater. 5 (2015) 1500124.
- [32] X. Ji, K.T. Lee, L.F. Nazar, Nat. Mater. 8 (2009) 500-506.
- [33] J. Cao, et al., Adv. Mater. 28 (2016) 9629-9636.
- [34] Z. Gao, et al., Nano Lett. 15 (2015) 8194-8203. [35] N. Li, et al., Chem. Commun. 48 (2012) 4106-4108.
- [36] G. Zhou, et al., ACS Nano 7 (2013) 5367–5375.
- [37] K. Xi, et al., Nanoscale 6 (2014) 5746-5753.
- [38] G. Hu, et al., Adv. Mater. 28 (2015) 1603-1609.
- [39] K.S. Novoselov, et al., Proc. Natl. Acad. Sci. 102 (2005) 10451-10453.
- [40] A.K. Geim, K.S. Novoselov, Nat. Mater. 6 (2007) 183–191.
- [41] T. Liu, et al., J. Mater. Chem. A 5 (2017) 17848-17855.
- [42] X. Wang, et al., Mater. Des. 139 (2018) 372–379.
- [43] C. Wang, et al., Polymer 131 (2017) 263–271.
- [44] B. Song, et al., Dalton Trans. 46 (2017) 15769–15777.
- [45] F. Ran, X. Yang, L. Shao, Adv. Compos. Hybrid Mater. 1 (2018) 32–55.
 [46] L. Ji, et al., Adv. Energy Mater. 6 (2016) 1502159.

- [47] K.R. Paton, et al., Nat. Mater. 13 (2014) 624–630.
 [48] Y. Zhang, L. Zhang, C. Zhou, Acc. Chem. Res. 46 (2013) 2329–2339.
- [49] J. William, S. Hummers, R.E. Offeman, J. Am. Chem. Soc. 80 (1958) 1339.
- [50] S. Stankovich, et al.. Carbon 44 (2006) 3342–3347
- [51] D.A. Dikin, et al., Nature 448 (2007) 457-460.
- [52] D.C. Marcano, et al., ACS Nano 4 (2010) 4806–4814.
- [53] A.A. Balandin, et al., Nano Lett. 8 (2008) 902-907.
- [54] C. Lee, et al., Science 321 (2008) 385-388.
- [55] H.J. Peng, J.Q. Huang, Q. Zhang, Chem. Soc. Rev. 46 (2017) 5237-5288.
- [56] F. Bonaccorso, et al., Science 347 (2015) 1246501.
- [57] K. Haubner, et al., ChemPhysChem 11 (2010) 2131–2139.
- [58] Y. Zhu, et al., Adv. Mater. 22 (2010) 3906-3924.
- [59] W. Gao, Graphene Oxide, Springer International Publishing, 2015.
- [60] M. Yu, et al., Energy Storage Mater. 1 (2015) 51-73.
- [61] S. Wu, et al., Nano Energy 15 (2015) 379-405.
- [62] Y. Zhao, et al., Nat. Commun. 5 (2014) 4565.
- [63] T. Lin, et al., Energy Environ. Sci. 6 (2013) 1283.
- [64] Q. Zhang, et al., Nano Lett. 15 (2015) 3780-3786.
- [65] L. Ji, et al., J. Am. Chem. Soc. 133 (2011) 18522-18525. [66] L. Zhang, et al., Phys. Chem. Chem. Phys. 14 (2012) 13670–13675.
- [67] K.C. Wasalathilake, et al., RSC Adv. 8 (2018) 2271–2279.[68] J. Park, et al., Adv. Energy Mater 7 (2017) 1700074.
- [69] K. Xi, et al., Chem. Commun 49 (2013) 2192-2194.
- [70] R. Chen, et al., APL Mater. 2 (2014) 124109.
- [71] H.J. Peng, et al., ACS Nano 8 (2014) 11280-11289.
- [72] G. Li, et al., Nat. Commun. 7 (2016) 10601.
- [73] G. Zhou, et al., Nano Energy 11 (2015) 356-365.
- [74] Y. Zhang, et al., Electrochim. Acta 222 (2016) 1257-1266.
- [75] R. Raccichini, et al., Nat. Mater. 14 (2014) 271-279.
- [76] J. Song, et al., Adv. Funct. Mater. 24 (2014) 1243-1250.
- [77] J. Song, et al., Nano Lett. 16 (2016) 864-870.
- [78] Z. Ma, et al., Angew. Chem. Int. Ed. 54 (2015) 1888-1892.
- [79] H. Wu, et al., J. Mater. Chem. A 5 (2017) 20458–20472.
- [80] Z. Xiao, et al., ACS Nano 11 (2017) 8488-8498.
- [81] M.R. Kaiser, et al., ACS Nano 11 (2017) 9048-9056.
- G. Zhou, et al., Nat. Commun. 6 (2015) 7760.
- [83] S.A. Ahad, et al., Electrochim. Acta 246 (2017) 451-458. [84] Z. Wang, et al., Nat. Commun. 5 (2014) 5002.
- [85] L. Zhou, et al., J. Mater. Chem. A 2 (2014) 5117-5123.
- [86] N. Xu, et al., Nano Lett. 17 (2017) 538-543.
- [87] R. Chen, et al., Nano Lett. 13 (2013) 4642-4649.
- [88] Z. Zhang, et al., Adv. Energy Mater. 7 (2017) 201602543. [89] M. Yu, et al., Energy Environ. Sci. 9 (2016) 1495-1503.
- [90] S. Bai, et al., Nat. Energy 1 (2016) 16094.
- [91] A.J. Blake, et al., J. Nanometer (2015) 212938.
- [92] J. Xu, et al., ACS Nano 8 (2014) 10920-10930.
- [93] B. Meyer, Chem. Rev. 76 (1976) 367–387.
- [94] J.Z. Wang, et al., J. Power Sources 196 (2011) 7030-7034.
- [95] Y. Zhang, Z. Gao, X. Li, Small 13 (2017) 1701927.
- [96] F. Zhang, et al., J. Mater. Chem. 22 (2012) 11452-11454.
- [97] Y. Cao, et al., Phys. Chem. Chem. Phys. 13 (2011) 7660-7665.
- [98] H. Wang, et al., Nano Lett. 11 (2011) 2644-2647.
- [99] S. Evers, et al., Chem. Commun. 48 (2012) 1233-1235. [100] H. Xu, et al., J. Mater. Chem. A 1 (2013) 15142-15149.
- [101] J. Zhang, et al., J. Power Sources 270 (2014) 1-8. [102] M.R. Sovizi, et al., New J. Chem. 41 (2017) 12589-12595.
- [103] C. Zhang, et al., Adv. Energy Mater. 4 (2014) 1301565.
- [104] L. Fei, et al., Adv. Mater. 27 (2015) 5936-5942.
- [105] H. Chen, et al., Nano Lett. 15 (2015) 798-802. [106] Y. Fu, et al., J. Am. Chem. Soc. 135 (2013) 18044-
- [107] D. Sun, et al., Nano Energy 26 (2016) 524-532.
- [108] C. Wang, et al., Nano Lett. 15 (2015) 1796-1802. [109] Y. Hwa, et al., Nano Lett. 15 (2015) 3479-3486.
- [110] K. Han, et al., J. Power Sources 251 (2014) 331-337.
- [111] B. Ding, et al., J. Mater. Chem. A 1 (2013) 1096–1101.

[112] H. Chen, et al., Nano Lett. 15 (2015) 5443-5448. [113] X. Wang, et al., J. Power Sources 242 (2013) 65-69. [114] J.Q. Huang, et al., Nano Energy 2 (2013) 314-321. [115] M. Yu, et al., Nanoscale 7 (2015) 5292-5298. [116] S. Li, et al., Electrochem. Solid State Lett. 14 (2011) A105-A107. [117] J. Jin, et al., RSC Adv. 3 (2013) 2558–2560. [118] Y. Zhang, et al., Nanoscale Res. Lett. 9 (2014) 137. [119] C. Tang, et al., Adv. Funct. Mater. 26 (2016) 577–585. [120] Z. Zheng, et al., Adv. Funct. Mater. 26 (2016) 8952-8959. [121] Z. Lyu, et al., Nano Energy 12 (2015) 657–665. [122] H. Yu. et al., Nano Res. 10 (2017) 2495-2507. [123] M.O. Zhao, et al., Nat. Commun. 5 (2014) 4410. [124] J. Shi, et al., Small 11 (2015) 5243–5252. [125] J. Shi, et al., Carbon 92 (2015) 96–105. [126] H. Zhuang, et al., RSC Adv. 7 (2017) 5177–5182. [127] Y. Li, et al., J. Mater. Chem. A 2 (2014) 4528–4533. [128] G. Hao, et al., Adv. Mater. 29 (2017) 1702829. [129] H. Chen, et al., Adv. Energy Mater. 7 (2017) 1700051. [130] G. Xu, et al., Chem. Eng. J. 322 (2017) 454–462. [131] J. Shi, et al., J. Energy Chem. 27 (2018) 167-175. [132] C. Zu, et al., Adv. Energy Mater. 3 (2013) 1008–1012.
[133] M.S. Park, et al., Phys. Chem. Chem. Phys. 14 (2012) 6796–6804.
[134] Q. Liu, et al., Appl. Phys. Lett. 108 (2016) 141906. [135] Z. Wu, et al., Electrochim. Acta 224 (2017) 527-533. [136] J. Zhang, et al., Adv. Mater. 28 (2016) 9539–9544. [137] C. Wang, et al., Nano Energy 11 (2015) 678–686. [138] S. Lu, et al., Sci. Rep. 4 (2014) 4629. [139] C. Xu, et al., J. Power Sources 275 (2015) 22-25. [140] B. Papandrea, et al., Nano Res. 9 (2016) 240–248. [141] H. Li, et al., Nano Energy 12 (2015) 468–475. [142] H. Li, et al., Adv. Energy Mater. (2018) 1703438. [143] H. Yuan, et al., Energy Storage Mater. 10 (2018) 1-9. [144] M.K. Song, et al., Nano Lett. 13 (2013) 5891–5899. [145] C.H. Chang, et al., ACS Energy Lett. 3 (2017) 72–77. [146] Z. Gao, et al., Electrochim. Acta 246 (2017) 507-516. [147] C. Wang, et al., J. Mater. Chem. A 2 (2014) 5018-5023. [148] Y. Qiu, et al., Nano Lett. 14 (2014) 4821-4827. [149] J. He, et al., Mater. Today Energy 1-2 (2016) 11-16. [150] Y. Xie, et al., ACS Appl. Mater. Interfaces 7 (2015) 25202-25210. [151] T.Z. Hou, et al., Angew. Chemie Int. Ed. 56 (2017) 8178-8182. [152] G. Zhou, et al., Adv. Energy Mater. 6 (2016) 1503155. [153] Y.X. Wang, et al., J. Power Sources 244 (2013) 240-245. [154] F. Wu, et al., Part. Part. Syst. Charact. 31 (2014) 639-644. [155] B. Li, et al., Nano Lett. 15 (2015) 3073-3079. [156] X. Huang, et al., J. Mater. Chem. A 1 (2013) 13484-13489. [157] K. Chen, et al., Nano Res. 11 (2017) 1345-1357. [158] Z. Wu, et al., Macromol. Chem. Phys. 218 (2017) 1700357. [159] K. Zhang, et al., J. Mater. Chem. C 5 (2017) 9359-9369. [160] C. Lin, et al., Electrochim. Acta 260 (2018) 65-72. [161] L. Zhu, et al., Nano Energy 11 (2015) 746–755. [162] Y. Wu, et al., Mater. Lett. 137 (2014) 277–280. [163] J.Q. Huang, et al., Carbon 99 (2016) 624-632. [164] R. Li, et al., Phys. Chem. Chem. Phys. 18 (2016) 11104-11110. [165] S. Niu, et al., J. Power Sources 295 (2015) 182-189. [166] J. He, et al., J. Mater. Chem. A 3 (2015) 18605-18610. Y. Chen, et al., J. Phys. Chem. C 119 (2015) 10288-10294. [168] S. Yuan, et al., Adv. Sci. 2 (2015) 1500071. [169] Y. Hwa, et al., Nano Lett. 17 (2017) 7086–7094. [170] Y.L. Ding, et al., Adv. Funct. Mater. 26 (2016) 1112-1119. [171] J. Cai, et al., ACS Appl. Mater. Interfaces 9 (2017) 33876-33886. [172] C. Tang, et al., Adv. Mater. 26 (2014) 6100-6105. [173] S. Huang, et al., Nano Res. 11 (2017) 1731-1743. [174] M.Q. Zhao, et al., ACS Nano 6 (2012) 10759-10769. [175] K. Chen, et al., Adv. Funct. Mater. (2018) 1707592.

[176] W. Deng, et al., J. Mater. Chem. A 5 (2017) 13674-13682.

[178] F. Wu, et al., Nano Lett. 16 (2016) 5488-5494. [179] Z. Li, et al., Nano Energy 23 (2016) 15-26. [180] S. Liu, et al., J. Mater. Chem. A 3 (2015) 11395–11402. [181] X. Fang, et al., Adv. Mater. 28 (2016) 491-496. [182] H. Li, et al., Nanoscale 8 (2016) 2395-2402. [183] S. Niu, et al., J. Mater. Chem. A. 3 (2015) 20218–20224. [184] F. Qin, et al., Nano Energy 38 (2017) 137–146. [185] F. Pei, et al., Nat. Commun. 8 (2017) 482. [186] H.J. Peng, et al., Adv. Funct. Mater. 24 (2014) 2772–2781. [187] Z. Gao, et al., Mater, Res. Lett. 5 (2017) 69–88. [188] M. Yu, et al., Mater. Chem. A 3 (2015) 9609–9615. [189] L.Q. Lu, et al., J. Mater. Chem. A 1 (2013) 9173-9181. [190] W. Zhou, et al., ACS Nano 7 (2013) 8801–8808. [191] Y. Zhang, et al., Carbon 114 (2017) 8–14. [192] Y. Liu, et al., Appl. Surf. Sci. 324 (2015) 399–404. [193] B. Li, et al., RSC Adv. 7 (2017) 54453–54459. [194] Y. Dong, et al., Nanoscale 7 (2015) 7569–7573. [195] P. Xiao, et al., Adv. Mater. 29 (2017) 1703324. [196] Y. Zhang, et al., J. Electrochem. Soc. 160 (2013) A1194—A1198. [197] L. Li, et al., ACS Appl. Mater. Interfaces 6 (2014) 15033-15039. [198] X.Y. Zhao, et al., Electrochim. Acta 113 (2013) 256-262. [199] C.Y. Chen, et al., Adv. Mater. 29 (2017) 1606802. [200] L. Zhang, et al., J. Electrochem. Soc. 164 (2017) H1086—H1090. [201] L. Zhang, et al., J. Electrochem. Soc. 164 (2017) H651—H656. [202] X. Lou, et al., ChemElectroChem 3 (2017) 3171—3180. [203] W. Bao, et al., Chem. Eur J. 23 (2017) 12613-12619. [204] X. Hong, et al., J. Alloys Compd 749 (2018) 586-593. [205] Y. Song, et al., ACS Appl. Mater. Interfaces. 10.1021/acsami.8b02920. [206] X. Huang, et al., J. Power Sources 356 (2017) 72-79. [207] Q. Pang, et al., Adv. Energy Mater 7 (2017) 1601630. [208] Z. Sun, et al., Nat. Commun. 8 (2017) 14627. [209] H.J. Peng, et al., Angew. Chem. Int. Ed. 128 (2016) 13184–13189. [210] Z. Yuan, et al., Nano Lett. 16 (2016) 519-527. [211] Y.S. Su, et al., Nat. Commun. 3 (2012) 1166. [212] Y.S. Su, et al., Chem. Commun 48 (2012) 8817-8819. [213] L. Xing, et al., J. Power Sources 303 (2016) 22-28. [214] Z. Xiao, et al., Adv. Mater 27 (2015) 2891-2898. [215] X. Liang, et al., Nat. Commun. 6 (2015) 5682. [216] P. Guo, et al., Electrochim. Acta 256 (2017) 28-36. [217] Y. Fan, et al., Adv. Energy Mater. 7 (2017) 1602380. [218] J. Xie, et al., Angew. Chem. Int. Ed. 129 (2017) 16441-16445. [219] W. Liu, et al., Proc. Natl. Acad. Sci. 114 (2017) 3578-3583. [220] J.Q. Huang, et al., ACS Nano 9 (2015) 3002-3011. [221] P. Zhu, et al., Carbon 126 (2018) 594-600. [222] H.J. Peng, et al., Adv. Sci. 3 (2016) 1500268. [223] Y. Zhao, et al., Nano Energy 30 (2016) 1-8. [224] J. Zhu, et al., Carbon 101 (2016) 272-280. [225] P.Y. Zhai, et al., Energy Storage Mater. 7 (2017) 56–63. [226] J. Li, et al., Mater. Lett. 139 (2015) 429–432. [227] T. Zhou, et al., Energy Environ. Sci. 10 (2017) 1694–1703. [228] T.Z. Zhuang, et al., Small 12 (2016) 381-389. [229] G. Zhou, et al., Adv. Mater. 26 (2014) 625-631. [230] X. Yao, et al., Adv. Energy Mater. 7 (2017) 1602923. [231] J. Zhao, et al., Nat. Nanotechnol. 12 (2017) 993-999. X.B. Cheng, et al., ACS Nano 9 (2015) 6373-6382. [233] H.J. Peng, et al., Adv. Energy Mater. 7 (2017) 1700260. [234] S.S. Zhang, Electrochim. Acta 70 (2012) 344-348. [235] A. Rosenman, et al., J. Electrochem. Soc. 162 (2015) A470-A473. [236] H. Pan, et al., Nat. Energy 2 (2017) 813-820. [237] R. Cao, et al., Adv. Energy Mater. 5 (2015) 1402273. [238] Y. Zhang, et al., ACS Energy Lett. 2 (2017) 2696-2705. [239] W. Li, et al., Nat. Commun. 6 (2015) 7436. [240] X.B. Cheng, et al., Adv. Mater. 28 (2016) 2888-2895.

[177] G. Zhou, Y. Zhaoa, A. Manthiram, Adv. Energy Mater 5 (2015) 1402263.